Netherlands organization for applied scientific research

TNO-report

report no. FEL-91-B112

copy no. 9

FEL

TNO Physics and Electronics Laboratory

P.O. Box 96864
2509 JG The Hague
Oude Waalsdorperweg 63
The Hague, The Netherlands

Fax +31 70 328 09 61
Phone +31 70 326 42 21

1

title

Radio channel measurements using a broadband Pseudo-Noise signal (measurement set-up and processing of the results)

author(s):

Ir. J.A.M. Vriens

Ir. G.J.M. Janssen

date:

June 1991

classification	
title	: unclassified
abstract	: unclassified
report text	: unclassified
appendices A/C	: unclassified

no. of copies	: 25
no. of pages	: 99 (incl. appendices, excl. RDP + distribution list)
appendices	: 3

TNO

report no. : FEL-91-B112

title : Radio channel measurements using a broadband Pseudo-Noise signal (measurement set-up and processing of the results)

author(s) : Ir. J.A.M. Vriens, Ir. G.J.M. Janssen

institute : TNO Physics and Electronics Laboratory

date : June 1991

NDRO no. :

no. in pow '91 : 711.2

Research supervised by:

Research carried out by:

ABSTRACT (UNCLASSIFIED)

In a multipath communications environment, which is often found in urban areas, transmission of information is difficult due to self-interference. This self-interference may result in signal suppression and intersymbol interference. Knowledge of the parameters that characterize the radio channel, can be used to feed an adaptive equalizer or frequency management system, in order to minimize these disturbing effects.

In this report a measurement system, to measure the characteristics of radio paths in a multipath channel, is described and measurement results are given.
The measurement system uses Pseudo-Noise Spread Spectrum modulation and operates in the VHF-band (30 - 70 MHz). A carrier, BPSK modulated with the Pseudo-Noise signal at a rate of 1 Mchip/s, is used to sound the radio channel.
The characteristics of the different radio paths: relative amplitude, RF-phase and delay-time, are calculated from the coherently received signal.

The accuracy of the measurement system has been determined and is: 2 dB for the amplitude, 5^{o} for the RF-phase and 20 ns for the delay-time.

With the system measurements have been performed in a controlled multipath environment in the laboratory and in the field in different types of terrain. The controlled multipath results are presented in this report, the analysis of the measurements performed in different types of terrain will be presented in [Vriens, 1991].

rapport no.	:	FEL-91-B112
titel	:	Radio kanaalmetingen door middel van een breedbandig Pseudo-Noise signaal (meetopstelling en verwerking van de meetresultaten).
auteur(s)	:	Ir. J.A.M. Vriens, Ir. G.J.M. Janssen
instituut	:	Fysisch en Elektronisch Laboratorium TNO
datum	:	juni 1991
hdo-opdr.no.	:	
no. in lwp '91	:	711.2
Onderzoek uitgevoerd o.l.v.	:	
Onderzoek uitgevoerd door	:	

SAMENVATTING (ONGERUBRICEERD)

In een omgeving met meerweg radiopropagatie, zoals vaak in stedelijke omgevingen voorkomt, wordt het verzenden van informatie bemoeilijkt door zelf-interferentie. Deze zelf-interferentie kan resulteren in signaalonderdrukking en intersymboolinterferentie. Indien de parameters die het radiokanaal karakteriseren bekend zijn, kan deze informatie worden gebruikt voor het sturen van een adaptief egalisatiefilter of een frequentiemanagement systeem om zo de negatieve effecten te minimaliseren.

In dit rapport wordt een meetsysteem beschreven waarmee de karakteristieken van radiopaden in een meerwegomgeving kunnen worden gemeten. Tevens worden meetresultaten gegeven.
Het meetsysteem maakt gebruik van "Pseudo-Noise Spread Spectrum" modulatie en werkt in de VHF-band (30 - 70 MHz). Een draaggolf, BPSK gemoduleerd met het "Pseudo-Noise"-signaal (met een chip-rate van 1Mchip/s), wordt als zendsignaal gebruikt.
De karakteristieken van de verschillende radiopaden: relatieve amplitude, RF-fase en vertragingstijd, kunnen uit het coherent ontvangen signaal worden berekend.

De nauwkeurigheid van het meetsysteem is bepaald, en is: 2 dB voor de amplitude, 5^{o} voor de RF-fase en 20 ns voor de vertragingstijd.

Met het systeem zijn metingen uitgevoerd aan een gecontroleerde meerweg omgeving in het laboratorium en in het veld in verschillende typen terrein. De resultaten van de gecontroleerde meerweg omgeving worden in dit rapport gegeven. De analyse van de metingen uitgevoerd in verschillende typen terrein, zullen in [Vriens, 1991] worden gepresenteerd.

CONTENTS

1 INTRODUCTION

In todays communications the role of mobile communications is increasing rapidly. In a mobile communications environment however, the transmission channels are not optimum; operation has to be performed in a more or less severe multipath environment and among other interfering signals.

Propagation of radio signals between a transmitter and receiver strongly depends on the geometry of the radio channel environment. When multipath propagation occurs (which is caused by different mechanisms as: reflection, diffraction and scattering), the desired signal in general reaches the receiver via more than one propagation path. Due to the occurring differences in amplitude, delay-time and RF-phase of the different paths, the received signal will be strongly distorted or extinguish totally at certain frequencies, which makes communication difficult or impossible.

When the multipath characteristics are known, this information can be used to counteract these negative effects.
For high data rate digital transmission systems (e.g. trunk connections) the multipath information can be used to feed an adaptive equalizer.
For narrow band operation the multipath information can be used to calculate the frequency response of a multipath channel in order to choose the optimum frequency. For proper operation of the adaptive equalizer and in order to choose the optimum frequency, accurate channel information is necessary on relative amplitude, RF-phase and delay-time of the occurring multipath signals.

In this report a channel measurement technique is presented which makes it possible to measure the complex amplitudes and delay-times of the radio signals arriving via different propagation paths. The measurement system is designed to operate in the VHF (Very High Frequency) band from 30 - 70 MHz. The radio channel is sounded by means of a broadband Pseudo-Noise (PN) signal. At the receiver side, the complex amplitude and delay-time of the different paths can be determined by means of software implemented correlation techniques.

The measurements to be performed with the presented technique serve the following goals:

- To determine the statistical characteristics of the multipath radio channels (delay-time, amplitude) for different terrain types;
- To investigate the possibility of using multipath characteristics to feed an adaptive equalizer in high rate data links;
- To investigate the possibility of using multipath characteristics for evaluating the narrow-band communication possibilities over a wide frequency band.

In this report the following items will be discussed:

- In chapter 2 the model of the multipath radio channel, as used in this report, is defined.
- In chapter 3 different principles of channel measurement techniques are discussed and the broadband channel measurement technique, as used here, is described.
- In chapter 4 the Pseudo-Noise measurement technique is described in more detail.
- In chapter 5 the processing of the received signal, which has been implemented in software, is given.
- In chapter 6 the accuracy of this technique is investigated.
- In chapter 7 the analysis of the narrow band frequency response of the communication links under consideration is described.
- In chapter 8 the results of tests in a simulated multipath environment, are discussed.
- Finally conclusions and recommendations are given.

Results of the measurements which have been performed in different types of terrain, will be presented in [Vriens, 1991].

2 DEFINITION OF THE RADIO CHANNEL

Very often, especially in an urban environment, the propagation of radio signals between 2 points takes place via different paths; a direct path and one or more indirect paths. This is called multipath propagation. In figure 2.1 a multipath situation is sketched.

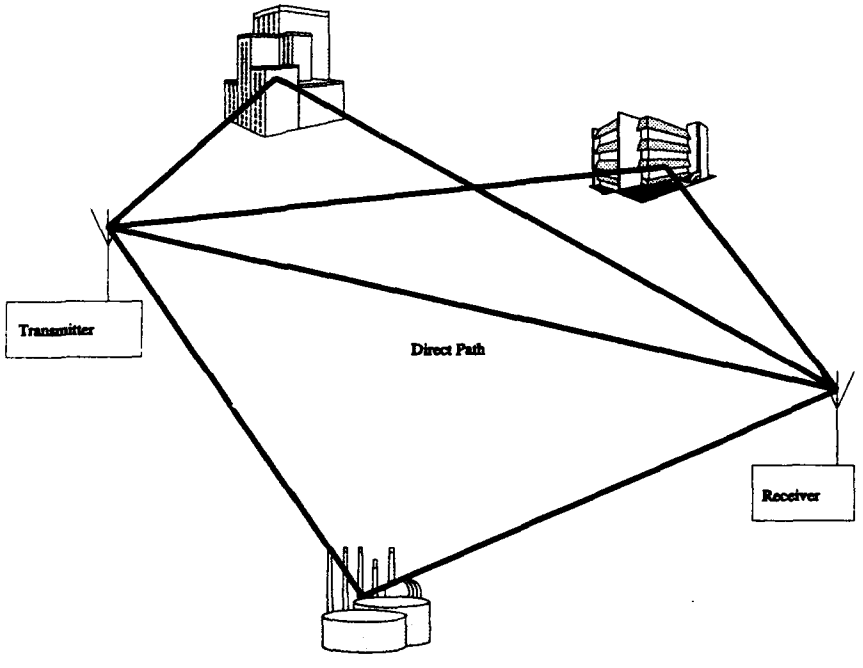

Fig. 2.1: A schematic view of a multipath channel

Different propagation effects that may play a role are: reflection, diffraction, delay-time, signal attenuation, etc.

When the radio channel consists of only one path, the radio signal is only attenuated and delayed. When the transfer function is frequency independent, no distortion will occur. However, in a multipath situation frequency dependent constructive and destructive interference will occur due to summation of different attenuated and delayed signal components. This may cause severe signal distortion or even total extinction of the signal.

When the multipath channel is known accurately over a broad frequency range, measures can be taken to improve communication possibilities. In broadband communication systems the distorting multipath effects can be compensated by using equalization. For narrow band systems optimum frequency selection, with maximum power transfer (constructive interference) is possible.

In multipath propagation a number of different mechanism play role. When all these mechanisms are taken into account, the description of the radio channel will become very complicated. Therefore a number of assumptions will be made for the model of the multipath radio channel that will be used throughout this report:

1. The multipath channel is a time independent radio channel. This is a valid assumption for communication systems with non-moving transmitter and receiver.
2. For a single path, propagation is assumed to be frequency independent. This means that attenuation and delay-time are assumed constant as function of frequency (no dispersion). This assumption results in a mayor simplification of the model. In practice, however, attenuation varies as 20log(f) with frequency. But for bandwidths within 10% of the carrier frequency it is a reasonable assumption.
3. The change of the RF-phase on different propagation paths as function of frequency, is only caused by the differences in path length (or delay-time).
4. To limit the number of paths in a practical multipath situation, only propagation paths with less than 30 dB attenuation, when compared to the strongest signal, are assumed to have a significant effect on the total channel response.

Based on these assumptions, the multipath channel can be modelled as the impulse response with complex transfer function h(t), which is the sum of the sub-transfer functions belonging to every single path:

$$h(t) = \sum_{i=1}^{N} h_i(t) = \sum_{i=1}^{N} A_i \exp(j\phi_i') \, \delta(t-\tau_i) \qquad (2.1)$$

Where A_i is the amplitude, ϕ_i' is the RF-phase shift due to reflections (in order to distinguish it from the phase shift due to the path delay-time τ_i), and τ_i the delay-time of the i^{th} path. $\delta(t-\tau_i)$ is the Dirac impulse function at instant τ_i. N is the number of relevant multipath channels.

When the complex transmitted and received signals are indicated as s(t) and r(t) respectively (with real parts $s_r(t)$ resp. $r_r(t)$ and imaginary parts $s_i(t)$ resp. $r_i(t)$), the signal arriving at the receiver for this type of channel is given by $r_r(t)$:

$$r_r(t) = \text{Real}\{s(t) * h(t)\} \qquad (2.2)$$
$$= \text{Real}\{\sum_{i=1}^{N} A_i \exp(j\phi_i') \, s(t-\tau_i)\}$$

which is the sum of attenuated, phase shifted and delayed versions of the original transmitted signal. Every single path propagates the signal undistorted.

If (2.2) is analysed it follows that the received signal is completely determined by the relative amplitude-, RF-phase- and delay-time values of the different paths in the multipath channel. Knowledge of these parameters allows a perfect prediction of the radio channel.
Theoretically this is true, however, in practice these parameters can only be determined with limited accuracy.
It will be shown that (with respect to the delay-time accuracy) for a good frequency response prediction over a reasonable bandwidth, it is sufficient to know the relative delay-time values with limited accuracy, when the relative RF-phase values of the multipath components are known accurately.

3 CHANNEL MEASUREMENT TECHNIQUES

Several measurement techniques exist to determine the multipath characteristics of a radio channel. These multipath characteristics are the number of relevant paths from transmitter to receiver and their respective amplitude, RF-phase and delay-time differences, as discussed in chapter 2. All paths together form the radio channel with impulse response h(t):

$$h(t) = \sum_{i=1}^{N} h_i(t) = \sum_{i=1}^{N} A_i \exp(j\phi_i')\delta(t-\tau_i) \qquad (2.1)$$

In order to measure the multipath characteristics of the radio channel, a number of techniques are available. In all these techniques the radio channel is sounded by a carrier signal, modulated with a specially chosen waveform, which makes it possible to distinguish the contributions of the different paths in the total received signal. In the following three broadband modulating waveforms will be discussed briefly:

- Pulse modulation,
- Frequency chirp wave modulation,
- Pseudo-Noise modulation,

3.1 Pulse modulation

With this technique a pulse of very short duration, modulated on a carrier signal, is transmitted. The complex transmitted signal can be indicated as:

$$s(t) = P(t)\exp(j\omega_c t) \qquad (3.1)$$

with:

- ω_c is the carrier frequency
- P(t) is the amplitude modulating pulse signal; $P(t) = U(t) - U(t-\tau_p)$
- U(t) is the unit step function
- τ_p is the duration of the pulse.

The actual transmitted signal is now:

$$s_r(t) = P(t)\cos(\omega_c t) \qquad (3.2)$$

With (2.2) it follows for the received signal:

$$r_r(t) = \text{Real}\{\sum_{i=1}^{N} A_i \exp(j\phi_i') P(t-\tau_i) \exp(j\omega_c(t-\tau_i))\} \qquad (3.3)$$

In the ideal case, this pulse has an infinitely short width and therefore occupies infinite bandwidth. If we assume that all paths have infinite bandwidth, for each path a similar response is received. The received signal may look like figure 3.1. From this figure the parameter values for the relative amplitude and delay-time can directly be derived.

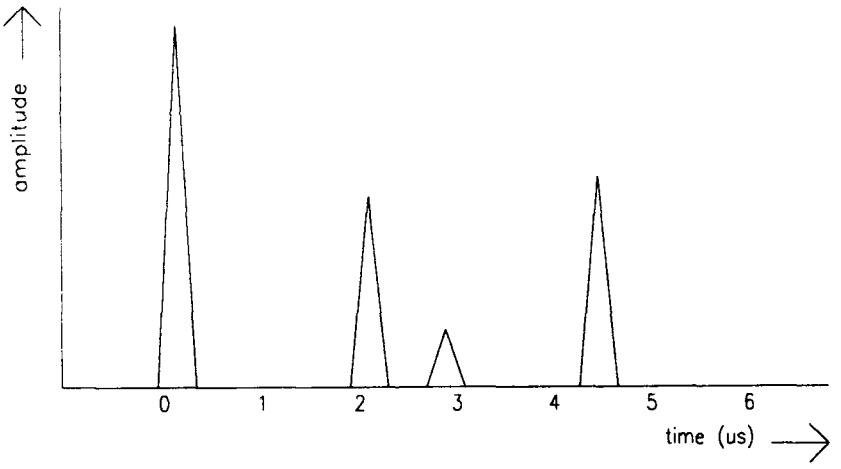

Fig. 3.1: Possible pulse response in case of 4 paths

In practice, however, several problems arise to implement this technique.
First, we cannot generate a pulse with infinitely short duration. Consequently, two paths may have a delay-difference less than the pulse duration and received pulses will interfere. In figure 3.2 this situation is depicted in case two path responses interfere. It takes more effort to separate the path delay-times of these pulses.

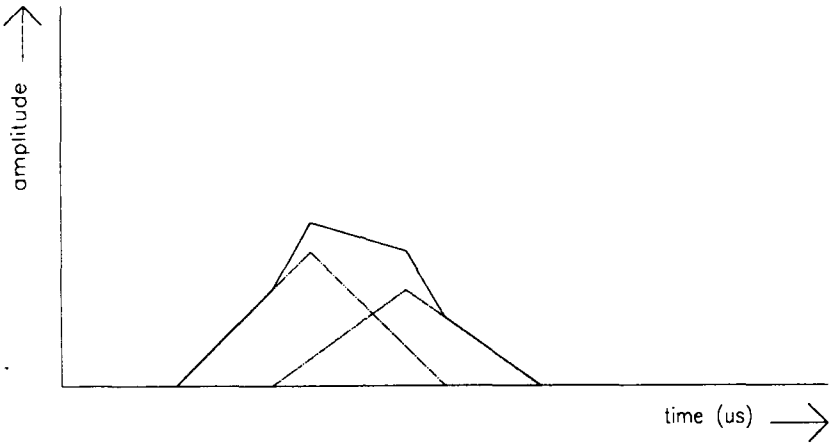

Fig. 3.2: Pulse response overlap due to multipath interference

In practice, the pulse will have a duration in the order of 1 microsecond. The pulse is rectangular and modulates a carrier at a certain frequency in the VHF-band. Depending on the exact pulse shape and duration, the pulse occupies a bandwidth of several megahertz, centred around the carrier frequency.

The second problem concerns the transmitter. Since the transmitted pulse has a very short duration, a large amount of energy must be concentrated in a very short time, in order to achieve a good signal-to-noise ratio at the receiver. Therefore, a very large peak power must be available at the transmitter. This puts high demands on the power amplifier of the transmitter.

The third problem with this technique concerns the receiver. Since most of the time only noise and no signal is present, the receiver must have a large dynamic range to process the unexpected pulse. Furthermore, the duration of the pulse makes it impossible to receive the signal coherently. Hence no phase information is detected and only the energy of each path instead of the complex amplitude can be determined.

3.2 Frequency chirp wave modulation

In this technique the transmitted signal is a carrier signal, which is periodically swept in frequency from ω_{min} to ω_{max}. The complex transmitted signal can be written as:

$$s(t) = \exp(j(\omega_{min} + \Delta t/2)t) \qquad (3.4)$$

with:

- Δ is the sweep rate $(\omega_{max} - \omega_{min})/T$ [rad/s^2]
- T is the sweep duration.

The signal arriving at the receiver is now:

$$r_r(t) = \mathrm{Real}\{\sum_{i=1}^{N} A_i \exp(j\phi_i')\exp(j(\omega_{min} + \Delta(t-\tau_i)/2)(t-\tau_i))\} \qquad (3.5)$$

When this signal at the receiver is demodulated with a carrier signal with the same sweep rate (e.g. the transmitted signal), this results in the signal component:

$$r_{rdem}(t) = \mathrm{Real}\{\sum_{i=1}^{N} A_i \exp(j\phi_i')\exp(j(-\omega_{min}\tau_i - \Delta t\tau_i + \Delta\tau_i^2/2))\} \qquad (3.6)$$

It is easily shown that the frequency difference between a multipath component and the actual transmitted frequency depends on the delay-time τ_i. For the i^{th} signal the frequency difference is $-\Delta\tau_i$, which is always smaller than the actual transmitted frequency.

In case there is only one path, one time-delayed version of the transmitted signal is received. Because of the frequency sweep, the delay-time corresponds to a certain frequency-decrease. Due to multipath effects, signals with different frequencies arrive at the receiver with different amplitude A_i, because the different paths have different amplitude transfer functions..

Each frequency component of the sum signal corresponds with a path delay-time. The frequency differences can be converted to delay-time differences of the different paths by:

$$\tau_2-\tau_1 = -(\omega_2-\omega_1)/\Delta \qquad (3.7)$$

Now from the frequency spectrum of the received signal the number of paths (signal components), their delay-time and attenuation can be determined. In figure 3.3 an example in case 2 paths with delay-time difference $\tau_2-\tau_1$ are received, is shown.

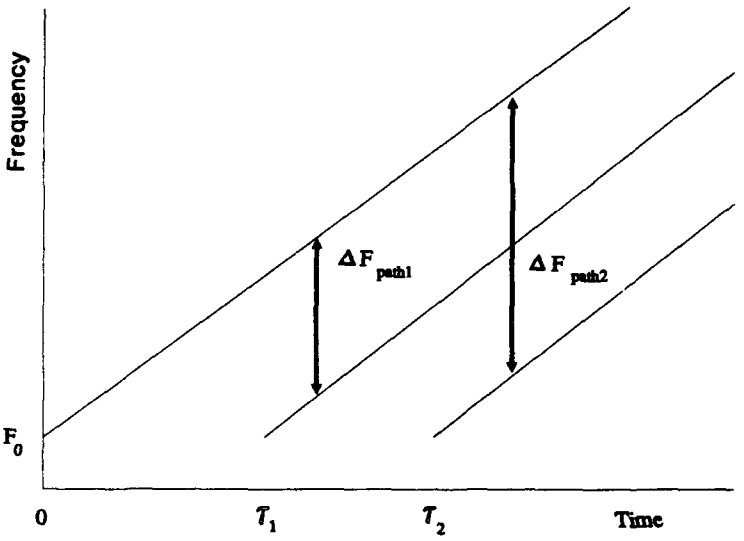

Fig. 3.3: *Frequency chirp wave modulation*

Since no coherent detection can be applied, no phase information is available. As for the broadband pulse measurements, only the energy of each frequency peak can be determined. But as distinct from the broadband pulse measurements, no special power requirements for the transmitter are necessary. Although the measurement occupies a wide frequency band, the instantaneous received and demodulated signal is a sum of narrow-band components which energy can be integrated over a sweep period. Therefore it is not necessary to transmit at very high power levels to achieve a reasonable signal-to-noise ratio at the receiver.

3.3 Pseudo-Noise sequence modulation

This technique is very close to the broadband pulse modulation technique as described in 3.1. However, two important problems are solved.
Instead of one pulse, a sequence of pulses is transmitted on a constant frequency. By correlation techniques, the responses of many pulses can be summed into one single pulse. This is possible because of the properties of the pseudo-noise sequence.
From the result after correlation the delay-times of the different paths can be determined, similar to the result obtained with the broadband pulse measurement technique. However, no high power transmitter is needed and by using a reference carrier signal at the transmitter frequency, coherent detection is possible so that the amplitude as well as the RF-phase of each path can be measured. Only the problem of pulse-interference caused by finite pulse-duration is still left.
Another advantage of this technique concerns the data processing. The received signal is a relatively long time-continuous signal which can easily be A/D-converted and stored on disc. Instead of real-time processing, the data can be processed at later instants. This makes it feasible to do more complicated data processing.

As modulating waveform for the measurement system, this PN-sequence modulation has been chosen, because it has the following advantages over other waveforms:

1. The transmitted signal is a low power signal.
2. The received signal is easy to detect coherently, which makes it possible to measure also the RF-phase differences between different paths.
3. This waveform is very useful for digital processing.

This technique will be described in more detail in the next chapter.
It will be shown there that PN-sequence modulation offers the principal possibility to regain the desired path parameters.

4 PSEUDO-NOISE SEQUENCE MODULATION AS CHANNEL MEASUREMENT TECHNIQUE

PN-code sequence modulation is a kind of direct sequence spread spectrum modulation, [Dixon, 1976].

In this chapter the properties of a specific class of PN-sequences, Maximum Length (ML) sequences, are discussed and the usefulness of PN-sequences as channel sounding waveform is shown.

Further, the measurement system and the design of the transmitter and receiver systems are described.

4.1 Theory of Pseudo-Noise sequences

The broadband channel measurement technique is based upon the correlation properties of the Pseudo-Noise (PN) sequence. The PN sequence consists of code bits, also called chips, whith assigned discrete values [-1, 1]. The length of a code chip is T_C, and $R_C = 1/T_C$ is called the chip rate.

The length of the sequence is K chips, after which it repeats itself again. The repetition time of the PN-sequence is $T_r = KT_C$.

There are different kinds of PN-code sequences. We have chosen for a Maximum Length code, which has some interesting properties for the use as channel sounding waveform:

1. It is easy to generate a Maximum Length (ML) code sequence.
2. The auto correlation has a well defined maximum value, which is reached within $2T_C$, elsewhere the auto correlation function has a constant low value.

4.1.1. A practical implementation to generate a PN-sequence

One property of a Maximum Length PN-sequence is that consecutive bits of the sequence are formed out of the last L bits. This relationship holds even after the last bit of the sequence e.g. the sequence starts over again. This type of PN sequences can be generated with a shift register generator. This generator consists of a number of shift registers for storage and shifting, and a number of modulo 2 adders called taps. Figure 4.1 shows a shift register generator of length L=10 with one tap [Holmes, 1982].

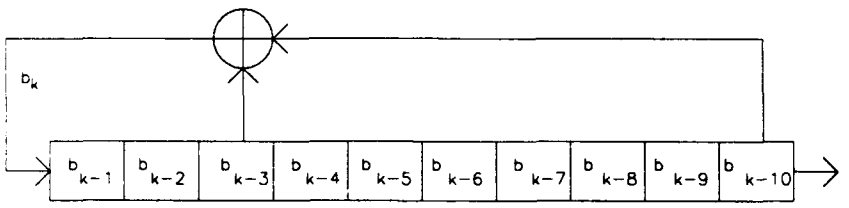

Fig. 4.1: Shift register generator for generating an ML PN-sequence

The output of the modulo 2 adders is fed back to the first stage of the shift register. Each clock pulse transfers the contents of stage j to stage j+1. The shift register sequence is defined to be the output of the last stage. The sequence is completely determined by the shift register length, the tap configuration and the initial contents of the shift register. The actual contents of the shift register $a_{k-1}\, a_{k-2} \,..\, a_{k-L}$ is referred to as the state of the system. We can describe the generated sequence by the fundamental linear recursion relation, relating the feedback sequence element a_k and the contents of the register:

$$a_k = c_1\, a_{k-1} \oplus c_2\, a_{k-2} \oplus \,..\, \oplus c_L\, a_{k-L} \qquad (4.1)$$

where $c_i \in \{0,1\}$ denotes the feedback relations. The symbol $\oplus$ stands for modulo 2 addition. The values $a_L\, a_{L-1} \,..\, a_1$ are termed the initial conditions.

For these shift register generators, all possible states except the all-zero state occur during sequence generation.
This special group of shift register generators are called a Maximal Length sequence generators because the length of the sequence equals the maximal number of different states except the all-zero state. Note that the all-zero state generates a sequence of length 1, and is transferred after each clock pulse into itself again. For a shift register of length L, a maximal length sequence has length K with

$$K = 2^L - 1. \qquad (4.2)$$

4.1.2 Definition of the auto-correlation function

To describe the correlation properties of ML-sequences we define both the continuous auto-correlation function $R(\tau)$ and the discrete auto-correlation function $R(m)$.
The continuous $R(\tau)$ auto-correlation function is given by:

$$R(\tau) = (1/KT_c) \int_0^{KT_c} PN(t)\,PN(t-\tau)\,dt \qquad (4.3)$$

The value of this function is [Holmes, Dixon]:

$$R(\tau) = \begin{cases} 1-(K+1)\,|\tau|/KT_c & \text{for } |\tau| < T_c \\ -1/K & \text{for } |\tau| > T_c \end{cases} \qquad (4.4)$$

So there is only one triangular correlation peak with width $2T_c$; elsewhere the correlation is constant with value, -1/K. A drawing of this function is given in figure 4.2.

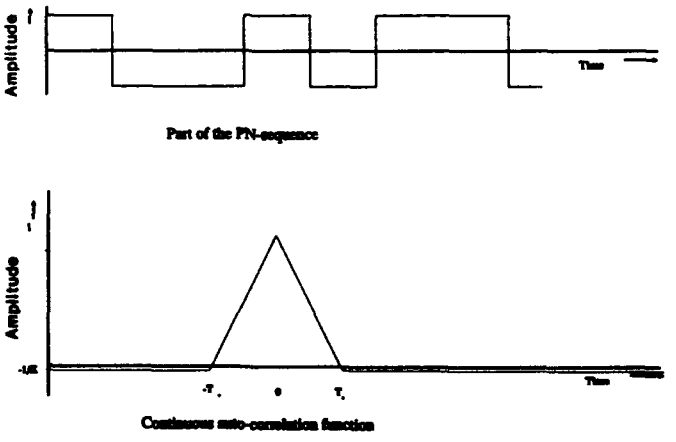

Fig. 4.2: Continuous auto-correlation function

The discrete auto-correlation function R(m) is slightly different. Let the symbols b_i of the maximal length sequence be $b_i = -1$ or $b_i = 1$, $i = 1,2, .. ,K$ and define modulo 2 addition according to:

$$-1 \oplus -1 = 1 \qquad (4.5a)$$

$$1 \oplus 1 = 1 \qquad (4.5b)$$

$$-1 \oplus 1 = -1 \qquad (4.5c)$$

$$1 \oplus -1 = -1. \qquad (4.5d)$$

Here we use the elements -1 and 1 instead of 1 and 0 respectively. Note that because of definition (4.5), the all-zero state is the state in which all stages of the shift register contains the element 1 rather than -1. By definition (4.5) the operation of modulo 2 addition equals multiplication. The discrete auto-correlation function of the sequence $b_1\, b_2 .. b_K$ is now given by:

$$R(m) = (1/p) \sum_{n=1}^{K} b_n\, b_{\{(n+m) \bmod K\}}. \qquad (4.6)$$

Since all, except the all-zero states are passed, the maximal length sequence contains $(2^L-1)/2 - 1$ times the element 1 and $(2^L-1)/2$ times the element -1. For $m \neq 0$, the auto-correlation function equals the sum of these elements divided by the sequence length according to (4.2). For exact overlap, m=0, the auto-correlation function becomes unity:

$$R(m) = \begin{cases} 1 & \text{for } m = 0 \\ -1/(2^L-1) = -1/K & \text{for } m \neq 0 \end{cases} \qquad (4.7)$$

The output of the discrete auto-correlation function is drawn in figure 4.3.

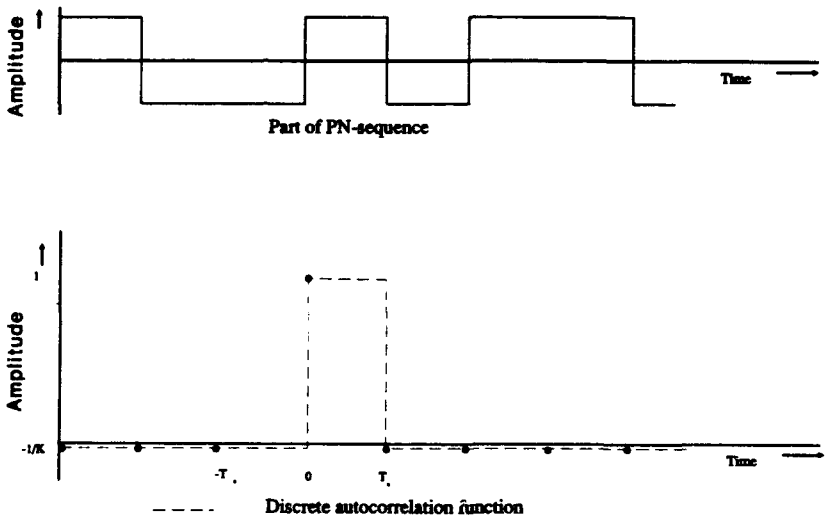

Fig. 4.3: The discrete auto-correlation function

The correlation function R has some important properties:

- The function has one maximum value, which has a triangular shape with width $2T_c$ for $R(\tau)$ and a square shape with width T_c for R(m). Outside the maximum value, the auto-correlation has a low constant value that depends on the sequence length. For the PN sequence generator of figure 4.1 the shift register has L = 10 stages so the ratio is $2^{10}-1 = 1023 \approx 30.1$ dB.
- Taking the correlation is a linear operation. Any version of the PN sequence, shifted in time or multiplied in amplitude, results in a similar correlation function with the same differences. The sum of any combination of N sequences will result in a similar sum of correlation functions.

4.1.3 PN-sequence modulation

A PN-sequence, which consists of code chips with the values [-1,+1], can be BPSK (Binary Phase Shift Keying) modulated on an RF-carrier signal and be transmitted. This transmitted signal can be written as:

$$s_r(t) = PN(t)\cos(\omega_c t) \tag{4.8}$$

The received signal in a multipath situation is now found with (2.2) to be:

$$r_r(t) = \text{Real}\{\sum_{i=1}^{N} A_i \exp(j\phi_i')PN(t-\tau_i)\exp(j(\omega_c(t-\tau_i))\} \tag{4.9}$$

$$= \sum_{i=1}^{N} A_i PN(t-\tau_i)\{\cos(\phi_i)\cos\omega_c t + \sin(\phi_i)\sin\omega_c t\}$$

where ω_c [rad/s] is the carrier frequency and ϕ_i is the resulting RF-phase shift $\phi_i = \phi_i' + \omega_c\tau_i$.
As indicated in 4.1.2, calculating the correlation of a signal is a linear operation. Therefore, the coherently demodulated multipath signal can, after correlation, be written as an In-phase signal $R_I(t)$ and Quadrature-phase signal $R_Q(t)$:

$$R_I(\tau) = \sum_{i=1}^{N} A_i . R(\tau-\tau_i) . \cos(\phi_i) \tag{4.10}$$

$$R_Q(\tau) = \sum_{i=1}^{N} A_i . R(\tau-\tau_i) \sin(\phi_i) \tag{4.11}$$

with $R(\tau)$ is the continuous correlation function of the PN-sequence with peak value at $\tau = 0$.
Now it can be seen that the amplitude and RF-phase information is contained in the I- and Q-output signals $A_i\cos(\phi_i)$ and $A_i\sin(\phi_i)$, of the coherent demodulator.
The above considerations show that correlation of the received PN-modulated signal with the same PN-code offers the principal possibility to regain the desired path parameters: relative amplitude, RF-phase and delay-time of the i^{th} propagation path.

4.2 The measurement system

In this section the measurement set-up and the signal waveforms that occur, are given. The practical realization of the measurement system is described in detail in [Feenstra, 1990].

4.2.1 Transmitter

Figure 4.4 shows a block diagram of the transmitter which is used to transmit the BPSK modulated PN-waveform. To realize the transmitted signal, we have used a far more complicated scheme but with this figure it is easy to explain the signal generation.

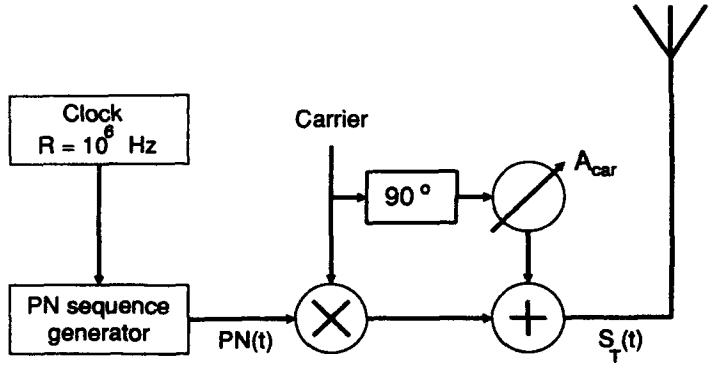

Fig. 4.4: Block diagram of the transmitter

4.2.1.1 Modulation of the PN-sequence

The PN sequence is generated by the shift register generator as given in figure 4.1, with a rate of $R_c = 10^6$ chips/second . The shift register has L = 10 stages so the PN sequence length is K = 2^{10}-1 = 1023. Upon the last bit the sequence starts over again. The output of the PN-sequence generator is a time continuous signal rather than a time discrete signal:

$$PN(t) = \sum_{n=1}^{\infty} b_n \, p(t-nT_c), \qquad (4.12)$$

with $T_c = R_c^{-1}$ the symbol duration time, the symbol shape p(t) is rectangular and given by:

$$p(t) = \begin{cases} 1 & \text{for } 0 \le t < T_c \\ 0 & \text{for } t < 0,\ t \ge T_c \end{cases} \qquad (4.13)$$

In (4.12) the element $b_n \in \{-1,1\}$ stands for symbol n of the PN sequence. The exact value can be determined with the fundamental linear recursive relationship for the PN sequence generator that is used:

$$b_k = b_{k-3} \oplus b_{k-10}. \qquad (4.14)$$

To start the sequence the initial conditions $b_1\ b_2\ ..\ b_{10}$ must differ from the all-zero state. Note that the upper index of the sum of (4.12) is ∞ rather than the length K = 1023 of the PN sequence. But since $b_k = b_k \bmod K$ with (4.12) an infinite sequence of consecutive PN sequences is denoted.

The time continuous PN sequence PN(t) is BPSK modulated on the transmitted signal, resulting in the signal (4.8):

$$s_r(t) = PN(t)\cos(2\pi f_c t) \qquad (4.8)$$

For each measurement the frequency f_c of this carrier is chosen in the VHF-band. The power spectrum of the PN-sequence is found to be [Ziemer and Peterson, 1985, p. 387]:

$$s_{PN}(f) = \sum_{m=-\infty}^{\infty} P_m \, \delta(f-mf_o), \qquad (4.15)$$

with $P_0 = 1/K^2$, $P_m = [(K+1)/K^2] \sin^2(mK/K)/(mK/K)^2$, K is the sequence length and $f_o = 1/KT_c$. Figure 4.5 shows the power spectrum of a PN sequence.

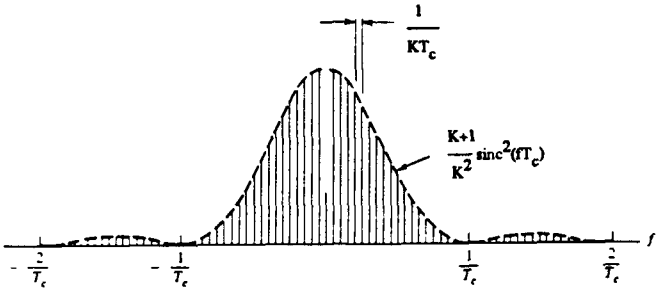

Fig. 4.5: The power spectrum of maximum length a PN sequence

Because of the periodicity of the sequence the spectrum has energy only at frequencies that are multiples of the reciprocal of the sequence duration time KT_c. The number of frequency components within one lobe equals the number of symbols K within one period of the PN sequence. Most of the energy of the sequence falls within $-T_c^{-1} < f < T_c^{-1}$. In our case $T_c = 10^{-6}$s and thus most energy is contained in a bandwidth of 2 MHz.

4.2.1.2 Addition of a reference carrier component

To be able to determine the complex amplitude, both in magnitude and RF-phase, the signal has to be detected coherently at the receiver. Therefore a reference carrier is needed at the receiver which is phase coherent with the transmitted signal. At the receiver this reference carrier must be recovered from the received signal.

Despite that the modulated PN sequence does not contain a carrier component, it is still possible to regain the carrier with a Costas-loop (Ziemer and Peterson, 1985, p. 261ff). But in practice the received signal to noise ratio turned out to be too low to have successful carrier regeneration with this Costas-loop. Furthermore the Costas-loop is very sensitive to interference.

For synchronization at the receiver we therefore transmit an unmodulated carrier component. This carrier is very narrow band and can therefore be filtered out easily with sufficient signal to noise ratio at the receiver. The filtered signal is then fed to a phase locked loop (PLL).

To let both symbols $b_i = -1$ or $b_i = +1$ have the same energy upon reception, the carrier component is mad- in quadrature phase by a 90 degree phase shift. With (4.8) the transmitted signal $s_k(t)$ finally becomes:

$$s_r(t) = PN(t)\cos(\omega_c t) + A_{car}\sin(\omega_c t), \qquad (4.16)$$

with $\omega_c = 2\pi f_c$ and f_c is the selected frequency in the VHF-band.

4.2.2 The Receiver

In figure 4.6 the block diagram of the receiver is shown.

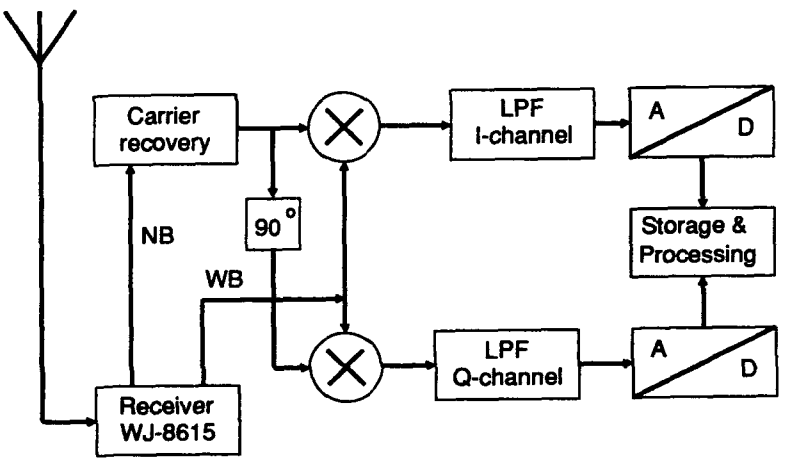

Fig. 4.6: Block diagram of the receiver

4.2.2.1 Demodulation

A local carrier transposes the received signal $r_r(t)$ to a fixed IF frequency band around $f=f_{IF}$. The resulting signal $r_{rIF}(t)$ is filtered twice.

A narrow band filter is used to filter out the added reference carrier component as described in section 4.2.1.2. The filtered output signal is used by a carrier recovery network (PLL) to regain the reference carrier signal. This carrier makes it feasible to detect the sequence PN(t) coherently. Because of the multipath characteristics of the radio channel, the reference carrier that is received is the sum of all carrier components that have propagated via different paths, and therefore have

different but constant RF-phases and amplitudes. So the recovered carrier has a constant RF-phase difference relative to the instantaneous phase of each path.

Beside the carrier component, the IF signal $r_{IF}(t)$ contains the responses of the PN signals of all paths and a noise term. This noise is assumed to be stationary white Gaussian noise with a two sided spectral density of No/2.
We are primarily interested in the determination of the amplitude A_i, RF-phase ϕ_i and delay-time τ_i of the i^{th} path.
Since the system is linear we continue the system description therefore by describing the demodulation of one single path. The total response is then found by addition of all individual path responses. The signal component of path i in the IF band is given by:

$$r_{IFi}(t) = A_i\ PN(t-\tau_i)\cos(\omega_{IF}t-\omega_c\tau_i-\phi_i') = A_i\ PN(t-\tau_i)\cos(\omega_{IF}t-\phi_i) \qquad (4.17)$$

with $\omega_{IF} = 2\pi f_{IF}$, $\phi_i = \omega_c\tau_i+\phi_i'$. ϕ_i' is the RF-phase of path i due to reflections and other mechanisms except path delay-time.

To limit the noise power, the signal $r_{IF}(t)$ is filtered by a 2 MHz wide filter, resulting for path i in the signal $r_{BIFi}(t)$. Because of the finite bandwidth of this filter, the spectrum of the PN-sequence is distorted slightly, and also some cross-talk to the quadrature channel occurs. The effect of cross-talk is that a signal which is in-phase with the reference carrier, will not only result in a signal in the in-phase channel, but also in the quadrature-channel.
This can be modelled in the following way. When a PN-modulated signal in-phase with the reference carrier is fed to the receiver, in the in-phase channel the almost undistorted (U) replica of the PN-signal will be found: $PN_U(t) \approx PN(t)$, whereas in the quadrature-channel a small but heavily distorted (D) PN-signal results: $PN_D(t) \approx 0$. The exact description of the filtered signal of (4.17) with cross talk components can now also be written as:

$$r_{BIFi}(t) = A_i\ (PN_U(t-\tau_i)\cos(\omega_{IF}t-\phi_i) + PN_D(t-\tau_i)\sin(\omega_{IF}t-\phi_i)) \qquad (4.18)$$

The signal $r_{BIF}(t)$ is fed to two mixers, driven by the regained reference carrier and a 90^o phase shifted version of this carrier. Since the two carriers form an orthonormal base in signal space, no information is lost by this operation. The mixers transpose the PN modulated signal from the IF band to the respective In-phase and Quadrature-phase baseband signals $r_{Ii}(t)$ and $r_{Qi}(t)$.
The higher frequency products are filtered out by the lowpass filters with impulse response $h_I(t)$ and $h_Q(t)$. These filters are almost equal, however, their responses $h_I(t)$ and $h_Q(t)$ are treated differently since slight differences in these responses influence the data processing results. Now let

$$A_{ci} = A_i/2 \cos(\phi_i), \tag{4.19}$$

$$A_{si} = A_i/2 \sin(\phi_i), \tag{4.20}$$

$$PN_{II}(t) = PN_U(t) * h_I(t), \tag{4.21}$$

$$PN_{QI}(t) = PN_D(t) * h_I(t), \tag{4.22}$$

$$PN_{IQ}(t) = PN_D(t) * h_Q(t), \tag{4.23}$$

$$PN_{QQ}(t) = PN_U(t) * h_Q(t), \tag{4.24}$$

where PN_{IQ} and PN_{QI} are the cross-talk components from the I- to the Q-channel and vice versa. These cross-talk components are very small.
By (4.19) and (4.20) the multipath parameters A_i and f_i for the amplitude and RF-phase of path i are replaced by A_{ci} and A_{si}, the amplitudes of the signal in the in-phase and quadrature-phase channels. The relations between A_i, f_i and A_{ci} and A_{si} are:

$$A_i = \sqrt{(A_{ci}^2 + A_{si}^2)} \tag{4.25}$$

$$\phi_i = \arctan(A_{si}/A_{ci}) \tag{4.26}$$

Now the baseband output signals are:

$$r_{Ii}(t) = A_{ci}PN_{II}(t-\tau_i) + A_{si}PN_{QI}(t-\tau_i), \tag{4.27}$$

$$r_{Qi}(t) = -A_{si}PN_{QQ}(t-\tau_i) + A_{ci}PN_{IQ}(t-\tau_i). \tag{4.28}$$

The symbol * denotes the convolution operation.

While the cross-talk components are very small, the essential terms of (4.27) and (4.28) for further calculations are those terms containing PN_{II} and PN_{QQ}.

4.2.2.2 Data sampling

The outputs of the filters, $r_I(t)$ and $r_Q(t)$, are fed to two independent A/D converters. Their output is stored on disc. In our system we record D = 8 consecutive PN sequences of K = 1023 bits each. The chip rate is 10^6 s^{-1} so one PN sequence lasts 1.023 ms. The duration of one measurement is 8.184 ms.

The resolution of the A/D converters is 8 bits/sample. This result in 256 amplitude levels.

For each symbol b_n of the PN sequence M = 8 samples are taken. Since the length of the PN sequence is K = 1023, the total number of samples per measurement is D.M.K = 8.8.1023 = 65,472.

We record 8 PN sequences instead of one sequence in order to be able to interleave the 8 corresponding samples of each sequence. By this interleaving operation the sample rate is increased virtually by a factor 8. The interleaving operation is described in the following chapter.

If the duration between 2 samples of the A/D converters is denoted by T_{AD} the recorded samples are described by:

$$I_n = r_I(nT_{AD}) \text{ for } n = 1,2,..,D.M.K, \qquad (4.29)$$

$$Q_n = r_Q(nT_{AD}) \text{ for } n = 1,2,..,D.M.K, \qquad (4.30)$$

Let us now observe the first 2 samples taken from PN sequence number 1.

If the sample rate would exactly equal a multiple of the transmitter bit rate and in the absence of noise, sample number 1+8K, the index of the first sample of the second PN sequence would be taken at the same instant as sample number 1. The sample rate $R_{AD} = T_{AD}^{-1}$ of the converters is chosen slightly lower from 8 times the chip rate R_c = 1 MHz (the exact sample rate is R_{AD} = 7.999878 MHz). This makes that equivalent samples of subsequent PN-sequences are taken 1/64 μs shifted in time so that the samples of the 8 sequences can be interleaved in the processing stage. This interleaving gives a virtual increase of the sample rate.

By using this technique we increase the sample rate virtually up to $64 . 10^6$ s^{-1}.

As described before, we can now add all path responses. Together with the noise terms, which are indicated as $n_I(nT_{AD})$ and $n_Q(nT_{AD})$, these signals form the samples stored on disc:

$$I_n = \sum_{i=1}^{N} A_{ci} PN_{II}(nT_{AD}-\tau_i) + A_{si} PN_{QI}(nT_{AD}-\tau_i) + n_I(nT_{AD}), \quad (4.31)$$

$$Q_n = \sum_{i=1}^{N} -A_{si} PN_{QQ}(nT_{AD}-\tau_i) + A_{ci} PN_{IQ}(nT_{AD}-\tau_i) + n_Q(nT_{AD}), \quad (4.32)$$

for n = 1,2,..,D.M.K. All noise samples are supposed to be statistically independent.

5 PROCESSING OF THE RECEIVED SIGNAL

In this chapter the processing of the received signal is described. The signal has been stored by means of the recorded samples on disc as discussed in chapter 4. The processing is performed by software on an AT personal computer, and consists of three parts:

1. Calculation of the correlation function;
2. Interleaving of the correlation functions;
3. Calculation of the multipath characteristics.

The calculations result in the desired parameters: relative amplitude, RF-phase and delay-time of all relevant paths. These results may then be transformed to the frequency domain to predict the narrow band frequency response of the radio channel, or used to feed an adaptive equalizer. When a large number of channels are measured, also statistical information can be gathered from the data for characterization of different types of terrain.

This part the data processing is described; for more detail on this subject see appendix B.

5.1 Calculation of the correlation function

The discrete auto-correlation function of the PN sequence has been calculated in chapter 4 and is found to be:

$$R(m) = (1/K)\sum_{n=1}^{K} b_n b_{(n+m) \bmod K} = \begin{cases} -1/(2^L-1) = -1/K & \text{for } m \neq 0 \\ 1 & \text{for } m = 0. \end{cases} \qquad (4.6)$$

where the symbols b_i i=1,2,..K represent the PN sequence.

There are a number of reasons not to use this correlation function (4.6) straight forward in our calculations.

1. The discrete correlation function (4.6) is a time-discrete function. The symbol index m corresponds with one chip duration time. In our system this time equals $T = 10^{-6}$ s.
   The delay-time differences that can be expected are of the same order of magnitude as the width of the correlation function. If correlation function (4.6) is used, it is not possible to distinguish paths with delay-time differences within the symbol duration time.

Since we want to be able to distinguish paths with delay-time differences as small as possible, 8 instead of 1 (and after interleaving 64) correlation function values per symbol are calculated.

2. The response of an occurring propagation path is contained in the samples from the I-phase as well as the Q-phase channel. The I- and Q-samples are processed separately. They contain the RF-phase information.

The duration of the correlation peak of each path should be as short as possible, in order to have minimum overlap between the correlation maxima belonging to different paths with almost equal delays. The length of this response partly depends on the function that is used to correlate the received samples. One of the input functions for the correlation operation is the sequence of the received samples. The other input function can be chosen so that the duration of the output correlation maximum is as short as possible.
The function that is used here, is chosen slightly different from the PN-code signal (which would result in a triangular correlation peak that is $2T_c$ wide). The signal has the same value as the PN-signal (+1 or -1) for the first sample period of a chip ($T = 1/8\ T_c$) and is zero elsewhere.
This function can be described by:

$$x_k = b_{\lceil (k)/MD \rceil}\, v_{((k-1) \bmod MD)} \quad \text{for } k = 1,2,.., \tag{5.1}$$

with v_k the discrete Dirac-function:

$$v_k = \begin{cases} 1 & \text{for } k = 0 \\ 0 & \text{for } k \neq 0. \end{cases} \tag{5.2}$$

The function $\lceil x \rceil$ denotes the smallest integer greater than or equal to x and $b_k \in \{-1,1\}$ is the PN sequence of (4.14).
The width of the correlation peak in this case is 1 μs. This is half the width of the correlation peak of the analog correlation function, where the width of the peak is 2 μs.
Both functions and the correlation function are depicted in figure 5.1.

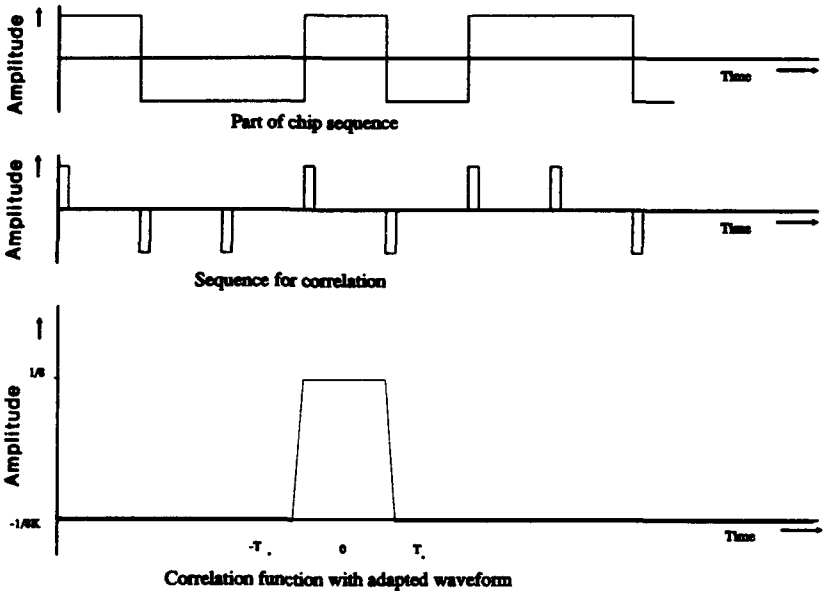

Fig. 5.1: Signals and correlation function

The calculation of the correlation functions of the received I- and Q- signals can now be described formally as:

$$R_I[n] = \sum_{k=-\infty}^{\infty} I[n+k]\ x[k], \qquad (5.3)$$

$$R_Q[n] = \sum_{k=-\infty}^{\infty} Q[n+k]\ x[k], \qquad (5.4)$$

with the notation $z[k]=z_k$ used to denote I[k], Q[k], and x[k] defined in (4.31), (4.32) and (5.1) respectively.

To clarify the correlation an example for a simplified case is calculated. In the simplified case only one path is received and the received samples exactly equal the transitted PN sequence. If we assume that the received signal and the regained carrier are in-phase, we may further disregard the quadrature channel. The received samples simply become:

$$I[k] = b[\lceil k/MD \rceil]. \tag{5.5}$$

With (5.1), (5.2) and (5.3) the correlation function is calculated:

$$\begin{aligned} R_I[n] &= \sum_{k=-\infty}^{\infty} x[k]\ I[n+k] \\ &= \sum_{k=-\infty}^{\infty} b[\lceil k/MD \rceil]\ v[(k-1) \bmod MD]\ b[\lceil (k+n)/MD \rceil] = \\ &= \sum_{j=-\infty}^{\infty} b[j+1]\ b[\lceil j+(1+n)/MD \rceil] = \\ &= \begin{cases} \sum_{j=-\infty}^{\infty} b[j+1]\ b[j+1] & \text{for } 0 \le n \le MD-1 \\ \sum_{j=-\infty}^{\infty} b[j+1]\ b[j+\lceil (1+n)/MD \rceil] & \text{for } n < 0,\ n > MD-1 = \end{cases} \\ &= \begin{cases} 1 & \text{for } 0 \le n \le MD-1 \\ -1/(2^L-1) & \text{for } n < 0,\ n > MD-1. \end{cases} \end{aligned} \tag{5.6}$$

The correlation function is an exact replica of one symbol response of the sequence I[k].
This correspondence is explained as follows: The received samples consist of consecutive symbol responses of the PN sequence. By taking the correlation, samples are added and subtracted. In case the received samples and the other input correlation function overlap, these values all contribute with the same sign e.g. positive signed samples are added and negative signed samples are subtracted. The result is an amplified value of one symbol response value.
In reality, the received samples will not equal the PN sequence as in (5.5) but they will be spread in time because of bandwidth limitations. In the resulting correlation function a similar time spread is found.

5.2 Interleaving of the correlation functions

The I- and Q- signals are sampled over a period of 8 consecutive PN-sequences. However, the moments of equivalent samples in two successive sequences are deliberately chosen not to coincide, as described in chapter 4. They are shifted over 1/8 of the sample period (1/64 μs). The same is true for the correlation functions. So the 8 consecutive correlation functions are all slightly shifted over 1/64 μs within one sample period. Now the correlation functions of the 8 sequences belonging to the same channel can be interleaved. This operation is shown in figure 5.2.

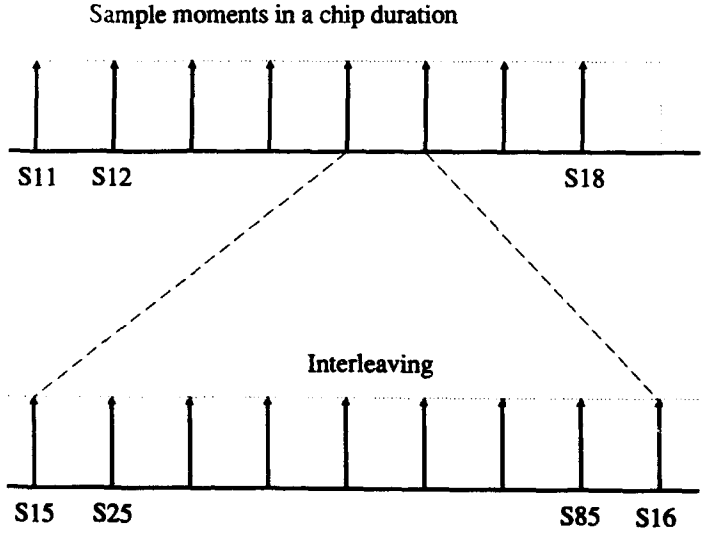

Fig. 5.2: Sampling- and interleaving operation

S_{15} indicates the fifth sample of the correlation function (the duration of which is about T_c) of PN sequence 1, S_{25} is the equivalent sample of PN sequence 2, , etc.
This results in an equivalent correlation function with an 8 times higher sample rate.

To remove the noise, the resulting correlation function is filtered with a moving average filter with length 8. The processing gain P_G (which is the improvement of the signal-to-noise ratio) of the correlation- and interleaving operations together is 10log(8.1023) = 39 dB.
Of course this can only be performed if the channel parameters don't vary in the observed time interval.
The advantages of this operation are:

- A higher virtual sample rate, resulting in an 8 times better time resolution,
  The system error is now 1/128 μs = +/- 7.8 ns.
- The signal independent noise contained in the samples of different sequences is uncorrelated and can be filtered out.

The new correlation function, after interleaving and filtering, is used to calculate the desired multipath parameters.

5.3 Calculation of the multipath characteristics

Calculation of the multipath characteristics from the I- and Q-correlation signals is quite complicated, and therefore, is given in full detail in appendix B. Here, only a qualitative description of these calculations is given.
The inputs for these calculations are the I- and Q-correlation functions and the reference I- and Q-correlation functions (Ref_I and Ref_Q; Ref_I contains information from PN_{II} and PN_{QI}, Ref_Q contains information from PN_{QQ} and PN_{IQ}). The reference correlation functions are determined by the transmitter and receiver parts of the system only. They are not dependent on the radio channel c.q. the multipath characteristics. These reference correlation functions which contain the influence of the transmitter and receiver characteristics due to filtering, phase shifting etc., are used to estimate the multipath characteristics. They are measured under laboratory conditions with transmitter and receiver directly connected together.

The calculated correlation functions of the received I- and Q-signals, $R_I[n]$ and $R_Q[n]$, are determined by:

- the multipath characteristics N, A_{ci}, A_{si} and l_i for i = 1,2,..,N,
- the noise terms,

as given in (5.3) and (5.4) with (4.31) and (4.32). l_i is the discrete delay-time value.

By chosing the right amplitudes A_{ci} and A_{si}, and delay-time l_i for path i, and assign these to Ref_I and Ref_Q, the newly formed $Ref_I(i)$ and $Ref_Q(i)$ can be matched with the received I- and Q-correlation signals belonging to path i.

We can now define the error criterium of the data processing to estimate the multipath characteristics: determine the number of paths N and for each path its amplitudes A_{ci}, A_{si} and delay-time l_i so that the energy contained in the remaining sample values in the I- and Q-channels is minimum. In other words: find N, A_{ci}, A_{si} and l_i for i=1,2,..,N so that

$$\Delta^2 = \sum_{n=-\infty}^{\infty} \{ R_I[n] - \sum_{i=1}^{N} A_I Ref_I[n-l_i] \}^2 + \sum_{n=-\infty}^{\infty} \{ R_Q[n] - \sum_{i=1}^{N} A_Q Ref_Q[n-l_i] \}^2, \qquad (5.7)$$

is minimum. Since the energy of $R_I[n]$ and $R_Q[n]$ is concentrated in the peaks of the function only, the summation of (5.7) can be restricted to a limited number of samples. This number must be determined first and will differ for each radio channel.

An iterating algorithm is used to determine the multipath characteristics. The block structure of the algorithm is shown by the flowchart given in figure 5.3.

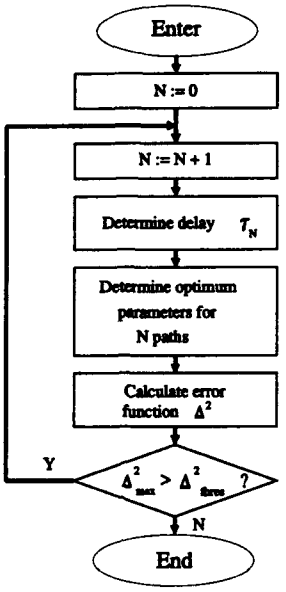

Fig. 5.3: Flowchart for the determination of the number of path and the path parameters

The algorithm starts with N=1 path and optimizes the amplitudes A_{c1} and A_{s1} and the delay-time l_1. With these parameters, which are assigned to the reference correlation functions $Ref_I[1]$ and $Ref_Q[1]$, the error Δ^2 of (5.7) is calculated. This error function is used to optimize the assigned path parameters.

When the parameters are optimum and the maximum value of the error function Δ^2, D_{max}^2, still exceeds a chosen threshold level, D_{thres}^2, the energy of the error function is supposed to originate from another path. In this case another path is added and the algorithm starts over again to find the optimum solution for both paths together.

Paths are added until the resulting maximum error D_{max}^2 becomes smaller than D_{thres}^2. The delay-time of the new extra path is determined by the maximum of the error function $\Delta^2[n]$.

The newly added path causes a decrease of the error function Δ^2 if the energy in D^2 originates from other paths of the radio channel. In case the energy of the error function is caused by received noise, the change of the error Δ^2 is undetermined. In practice it turns out that the error Δ^2 always decreases. Hence we may state that the algorithm converges.

The last step to obtain all multipath characteristics is the determination of the amplitude and RF-phase differences of the found paths from the amplitudes A_{ci} and A_{si}. These are already given in (4.25) and (4.26):

$$A_i = \sqrt{(A_{ci}^2 + A_{si}^2)} \qquad (4.25)$$

$$\phi_i = \arctan(A_{si}/A_{ci}). \qquad (4.26)$$

6 ACCURACY OF THE MEASURED PARAMETERS

From the channel-measurement results the relative amplitude, RF-phase and delay-time of the different multipath signals are determined by processing of the received signal as is presented in the previous chapters. How precise the characteristics of the radio channel can be estimated, depends on the accuracy of the measured path parameters.

In this chapter the accuracy of the measured parameters will be evaluated. The sources of error for the parameters are:

- amplitude: noise
- delay-time: noise, sample frequency
- RF-phase: noise, phase-jitter of the reference carrier.

In the following at first the signal-to-noise ratio, and the influence of phase-jitter of the reference carrier will be discussed. Then the effects of the error-sources on the accuracy of the path parameters will be evaluated.

6.1 Signal-to-Noise Ratio

The total received signal contains a signal part S, and a noise part, N_r (r = received). The SNR (Signal-to-Noise Ratio) of the received signal is defined as SNR = S/N_r.

The SNR of the received signal after A/D-conversion is determined by:

- the SNR of the received signal S/N_r,
- the quantization noise caused by A/D-conversion N_q (q = quantization).

- Influence of quantization noise

The influence of N_q can be determined by comparing the SNR before and after A/D-conversion. A/D-conversion is performed by an 8 bits converter. This means that the voltage range is subdivided into 256 steps. When the voltage range is used optimum, and N_r is assumed to be 0, the maximum SNR that can be reached is, [Carlson, 1975]:

$$SNR_{max} = S/N_q = 10*\log(3\cdot 256^2) = 53 \text{ dB}. \qquad (6.1)$$

Because N_r and N_q are independent, the total noise power after A/D-conversion is $N_{tot} = N_r + N_q$.

Now it can be shown easily that the influence of N_q on the total SNR becomes significant only when the SNR of the received signal S/N_r, is about 50 dB or higher. In practical field measurements such high S/N_r will not be common practice. More reasonable values are $S/N_r < 20$ dB. Then the influence of N_q is neglectable, and the SNR after the A/D-converter is approximately equal to S/N_r.

- SNR after signal correlation.

Up to now only the SNR before signal processing (correlation) has been investigated, however, the SNR will increase significantly after correlation. The effect of correlation and interleaving of 8 PN series results in a processing gain P_G of $P_G = 10\log(8.1023) = 39$ dB. So the SNR_C (SNR after correlation) of the signal which is used to determine the pulse position, is related to S/N_r by:

$$SNR_C = S/N_r + 39 \text{ dB}. \qquad (6.2)$$

In this result the influence of the processing gain is clearly demonstrated. Even with a low S/N_r the SNR_C can be quite good.

- Determination of the SNR_C for a single multipath component

For a given pulse shape, the time accuracy is determined by the SNR_C after correlation as will be shown in paragraph 6.3. SNR_C has to be determined for a single pulse (or path). For a single pulse S and N can be calculated as follows:

$$S = (T_p)^{-1} \int_0^{T_p} |p(t)|^2 \, dt \qquad (6.3)$$

$$N = (T_n)^{-1} \int_0^{T_n} n^2(t) \, dt \qquad (6.4)$$

Here T_p is the time interval of a the pulse, T_n is a time interval with no signal energy present.

6.2 Errors caused by phase-jitter of the reference carrier

In the signal processing phase, 8 successively received PN sequences are correlated independently. After correlation the results are interleaved. In the ideal situation a smooth curve will result with sample values at 1/64 μs distance. However, in practice it points out that the phase of the reference carrier is not stable. It contains a significant amount of jitter. This causes that the amplitude of the signals in the in-phase and quadrature-phase channels of the receiver are not stable in time.

An example of the resulting correlation peak after interleaving is given in figure 6.1.

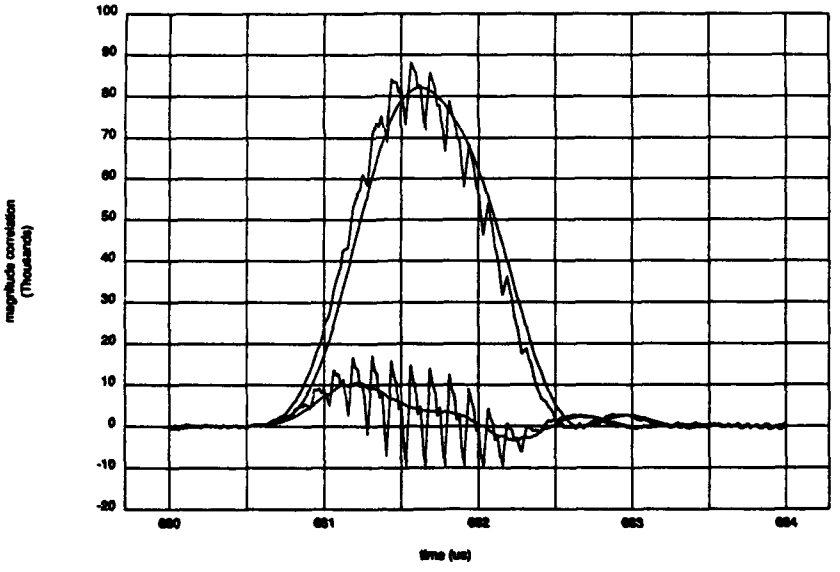

Fig. 6.1: Correlation peak, as calculated from measurement results, with the effect of phase-jitter (I, Q) and after moving-average filtering (I, Q)

By using a moving-average filter with length 8, the amplitude variations are filtered out (figure 6.1). By simulation the effects of these operations (interleaving with phase-jitter and filtering)

have been evaluated for different peak-peak phase-jitter values. It pointed out that phase-jitter of the reference carrier causes an amplitude error, but no RF-phase error.

6.3 Delay-time error

6.3.1 Delay-time errors due to noise

In the case of a radar signal, the time elapsed between the moment of transmission of the radar pulse and reception of the reflected signal determines the range to the origin of the reflection. In general the received signal is a distorted replica of the transmitted pulse embedded in noise. This causes that the measurement of the delay-time has not infinite accuracy.
The error in the delay-time of the correlation peak embedded in noise in our case is equivalent with the error in the echo-time of a radar signal in noise.
Therefore, calculations originating from the radar science [Woodward, 1953; Barton, 1969] can be used to determine the accuracy of the measured relative delay-times between the correlation peaks of the multipath components and the direct signal.

The delay-time accuracy that can be achieved depends on the SNR and the shape of the pulse. The accuracy will increase with increasing SNR and with increasing rise- and fall-times (which is equivalent with a larger spectral bandwidth of the signal) of the pulse.

A measure for the accuracy is the RMS (Root Mean Square) error σ_τ [s]. For a given pulse shape the minimum RMS-error is given by σ_τ, [Woodward, 1953; Barton, 1969]:

$$\sigma_\tau = 1/(\beta\sqrt{SNR_m}) . \qquad (6.5)$$

The received pulse energy is maximized when the receiver characteristics are matched to the pulse (matched filter receiver). For a matched filter receiver $SNR_m = 2E/N_0$ is the peak SNR; E is the energy in the received pulse and N_0 the spectral noise density. The variable β contains information about the pulse shape, it especially depends on the rise- and fall times of the pulse. β is given by:

$$\beta = \frac{\int_{-\infty}^{\infty} | \partial/\partial t \; P(t) |^2 \, dt}{\int_{-\infty}^{\infty} | P(t) |^2 \, dt} \qquad (6.6)$$

β is the RMS bandwidth of the pulse signal, P(t) is the complex pulse shape.

To be able to calculate the delay-time error due to noise, the SNR of the pulse signal has to be known. The receiver which has been developed to perform practical measurements, is an approximation of the matched filter receiver. Therefore the received SNR_s is sub-optimum, $SNR_s < SNR_m$. In the following it will be assumed that $SNR_s = SNR_m/2$ to compensate for mismatching.

In figure 6.2 the calculated standard deviation σ_τ of the delay-time error is given as function of SNR_C (SNR after correlation as discussed in paragraph 6.1) for the same pulse-shape as is used in the measurement system, for which $\beta = 1.86 \cdot 10^6$.

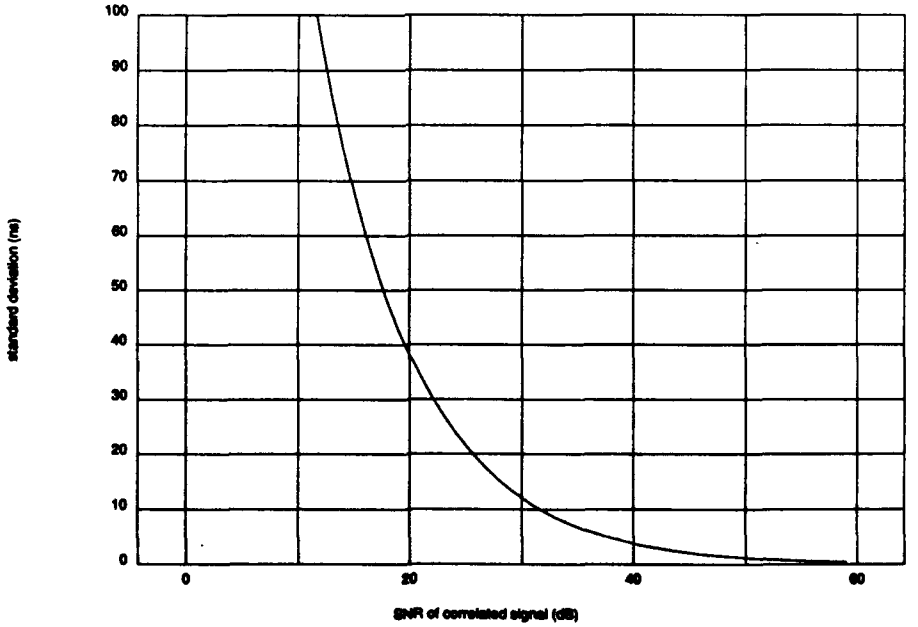

Fig. 6.2: The calculated standard deviation of the delay-time error as function of the input-SNR

6.3.2 Influence of the measurement method on the delay-time error

The effective sample time of the signal after correlation and interleaving is 1/64 us = 15.6 ns. The inherent error caused by this discretization is +/- 7.8 ns. Because the distribution of the discretization error is uniform, the standard deviation due to this error is 4.5 ns.

From fig. 6.1 it can be seen that for SNR_C > 45 dB (input-SNR > 6 dB), the standard deviation of the delay-time error is smaller than the system standard deviation of 4.5 ns. Both these error are independent, so the total variance is found by adding both variances.
For the delay-time between two correlation peaks (1 and 2), the variance in the relative delay-time is determined by the variances in the delay-times of both peaks (the errors are independent):

$$\sigma_{tot}^2 = \sigma_1^2 + \sigma_2^2 \qquad (6.7)$$

6.4 Amplitude error

In the chosen measurement set-up there are two causes of errors in the measured amplitude of a radio path.

1. Amplitude errors due to noise. The presence of the noise will cause a statistical deviation that depends on the SNR.
2. In the measurement set-up the reference carrier is recovered by means of a Phase Locked Loop (PLL). The reference carrier from the PLL still has some phase-jitter. Depending on the amount of jitter, this also causes amplitude errors.

6.4.1 Amplitude error due to noise

A carrier signal plus noise which is bandpass filtered can be written as a sum of an in-phase and a quadrature phase component.

$$s(t) = (A + n_I(t))\cdot\cos(\omega t) - n_Q(t)\cdot\sin(\omega t) =$$
$$= R(t)\ \cos(\omega t + \phi(t)) \qquad (6.8)$$

In this formula R(t) and ϕ(t) are:

$$R(t) = [\{A + n_i(t)\}^2 + \{n_q(t)\}^2]^{0.5} \quad (6.9)$$

$$\phi(t) = \arctan(\{n_q(t)\}/\{A + n_i(t)\}) \quad (6.10)$$

This equation relates the envelope and phase of a carrier plus bandpass noise to the signal and noise components. The probability density function (PDF) for R(t) and $\phi(t)$ is given by (Carlson, 1975):

$$p(R,\phi) = \frac{R}{2\pi N} \exp\{-(R^2 - 2AR\cos\phi + A^2)/2N\} \quad (6.11)$$

This is a joint PDF, and R and ϕ are statistically dependent.
For large SNR = $A^2/2N$ (where N is the noise power in the pass-band of the filter), the probability density function for the amplitude can be estimated by:

$$p_R(R) = (R/2\pi AN)^{1/2} \exp\{-(R-A)^2/2N\} \quad (6.12)$$

Now it follows for the mean deviation and variance of the amplitude (Carlson, 1975):

$$\bar{R} = A \quad (6.13)$$

$$\sigma_R^2 = N \quad (6.14)$$

With (6.14) the standard deviation of the amplitude error can be calculated as function of SNR_C.
In figure 6.3 the value $(A + \sigma_R)/A \approx 1 + 1/\sqrt{2}*SNR_C$ is given as function of SNR_C.

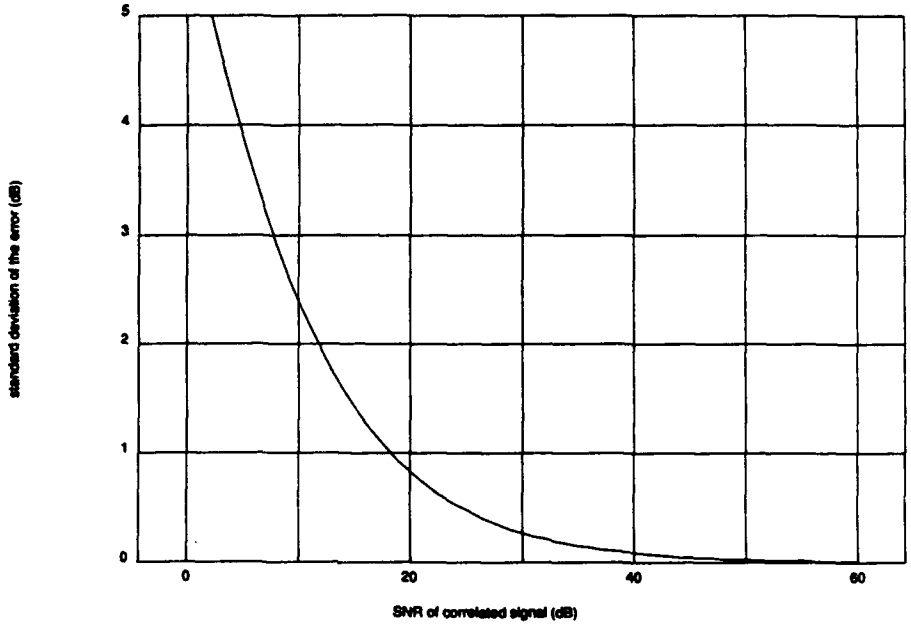

Fig. 6.3: The calculated standard deviation of the amplitude error due to noise

6.4.2 Amplitude error due to phase-jitter of the reference carrier

As discussed in paragraph 6.2, the phase-jitter of the reference carrier influences the signal that is received of the 8 successively transmitted PN-sequences. Computer simulation showed that this causes an amplitude error that depends on the peak-peak phase-jitter. The calculated amplitude error is given in figure 6.4. In practice the peak-peak phase-jitter of the reference carrier will be within 45 degrees, than the maximum error is within 0.5 dB.

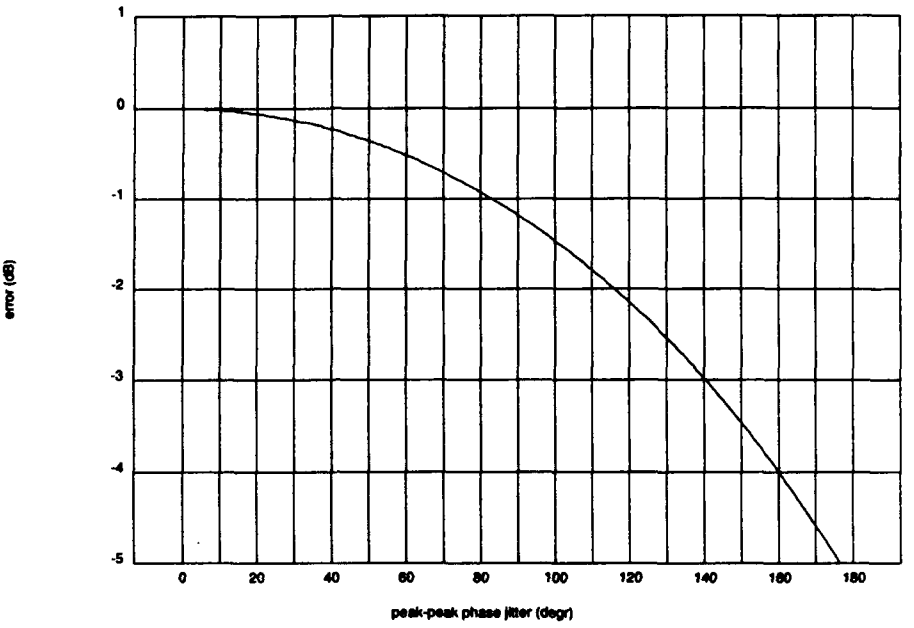

Fig. 6.4: The effect of phase-jitter on the amplitude error

6.5 RF-phase error

The calculated RF-phase related to the signal content of the I-and Q-channels, will deviate when noise is present. From the given joint PDF of the amplitude and phase as given in paragraph 6.2.1 , the PDF (Probability Density Function) of the phase error can be estimated for SNR >> 1 by:

$$P_{\phi}(\phi) = (A^2/2\pi N)^{1/2} \cos\phi \exp\{-(A^2 \sin^2\phi)/2N\} \qquad (6.15)$$

From this relation it follows for the mean error and the variance that:

$$\overline{\phi} = 0 \qquad (6.16)$$

$$\sigma_{\phi}^2 = N/A^2 \qquad (6.17)$$

In the same way as given in paragraph 6.4.1 the standard deviation of the RF-phase is calculated as function of SNR_C. The results are given in figure 6.5.

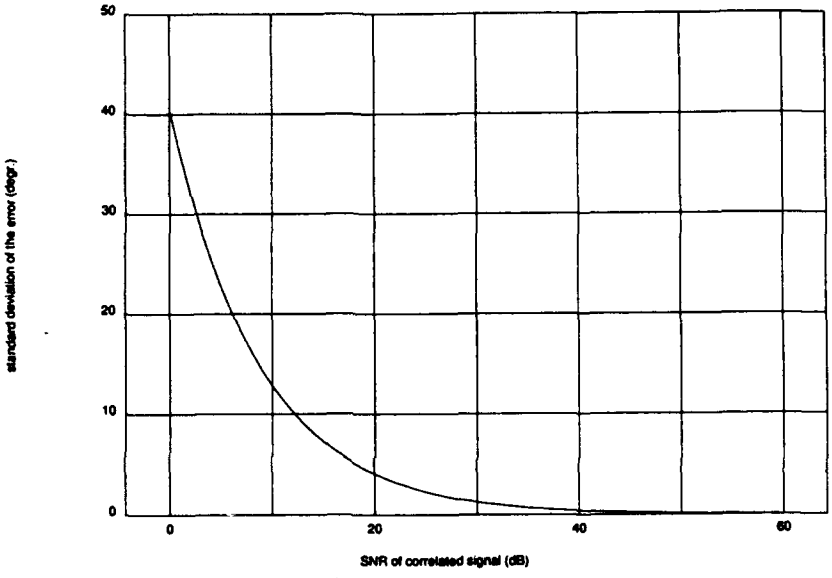

Fig. 6.5: The calculated standard deviation of the RF-phase error due to noise

For $SNR_C > 20$ dB, the standard deviation of the phase error < 5 degr.

6.6 Conclusion

The errors due to noise are very small. For a SNR_C = 25 dB (S/N_T = -14 dB), the standard deviations are:

- time : 22 ns
- amplitude : 0.5 dB
- RF-phase : 3 degr.

In general the input-SNR will be much higher so that the errors due to noise become very small.
With respect to the calculation of the delay-time, the systematic error is within +/- 7.8 ns.
Phase-jitter in the reference carrier causes only an amplitude error and no phase error. This error is not dependent on the RF-phase, it only depends on the peak-peak phase-jitter. For peak-peak phase-jitter = 30 degr. the amplitude error is 0.2 dB.

7 FREQUENCY RESPONSE OF THE RADIO CHANNEL

In this chapter the method that has been used to calculate the frequency response of a multipath radio channel, will be discussed. The parameters of the single paths in the radio channel, which can be measured and calculated as described in the previous chapters, are input for the calculations.
One of the problems that will be addressed is the influence of the uncertainty in the measured delay-times.

7.1 The frequency response

In chapter 2 the model of the multipath radio channel is discussed in detail. There the impulse response h(t) of the radio channel (2.1) is given:

$$h(t) = \sum_{i=1}^{N} h_i(t) = \sum_{i=1}^{N} A_i \exp(j\phi_i')\delta(t-\tau_i) \qquad (2.1)$$

where A_i is the amplitude, ϕ_i' the RF-phase and τ_i the delay-time of path i. N is the number of paths. The frequency response H(f) can be calculated by taking the Fourier transform from the impulse response h(t). H(f) is given by:

$$H(f) = \int_{-\infty}^{\infty} h(t)\exp(-2\pi jft)\,dt$$

$$= \sum_{i=1}^{N} A_i \exp\{-j(2\pi f\tau_i - \phi_i')\} \qquad (7.1)$$

H(f) is a complex function and is therefore described by its amplitude and phase. In stead of the amplitude, we will use here the power spectrum $S(f) = |H(f)|^2$. With (7.2) the power spectrum S(f) can be calculated from the path parameters.

$$S(f) = \{\sum_{i=1}^{N} A_i \cos(2\pi f\tau_i - \phi_i')\}^2 + \{\sum_{i=1}^{N} A_i \sin(2\pi f\tau_i - \phi_i')\}^2 \qquad (7.2)$$

The phase response as function of frequency is given by:

$$\phi(f) = \arctan(\{\sum_{i=1}^{N} A_i \cos(2\pi f\tau_i - \phi_i')\} / \{\sum_{i=1}^{N} A_i \sin(2\pi f\tau_i - \phi_i')\}) \qquad (7.3)$$

From (7.2) we can see that the power spectrum is frequency dependent because of the multipath effect. The variation in the received signal power caused by interference is determined by the amplitude A_i and delay-time τ_i of each path. The phase response $\phi(f)$, as given in (7.3), also deviates from the ideal linear case due to multipath.

For frequency management purposes the power spectrum S(f) contains all necessary information for narrow band signals. For this type of signals phase variation over the frequency band occupied by the signal, will be small. Therefore in the following only the power spectrum S(f) will be taken into account.

7.2 Influence of the delay-time accuracy

When calculating the frequency response from the path parameters, the phase at at certain frequency is determined by the measured RF-phase ϕ_i at the measurement frequency and the delay-time τ_i. The accuracy of τ_i is of great importance for the accuracy of S(f).

If we consider path j with delay-time τ_j the RF-phase of this path is periodical with $1/\tau_j$. The contribution of this path with amplitude A_j in (7.2) will changed from its minimum ($-A_j$) into its maximum value ($+A_j$) by a change of the phase by π rad.

The uncertainty of the delay-times has two main causes:

1. The finite sampling rate of $R_s = 64*10^6\ s^{-1}$ causes a discretization error of $\Delta t = 7.8125$ ns,
2. Noise.

At the frequency f = 50 MHz a phase shift of π rad is caused by a delay-time shift of $\Delta\tau_j = 10$ ns. This means that the uncertainty in the measured delay-times, which is in the order of 20 ns, is

about one period of the RF-signal in the frequency band 30 - 70 MHz, where the measurements are carried out.
In the following paragraph the effects of the delay-time inaccuracies will be shown and a method will be presented to partly compensate for these inaccuracies by changing the delay-times τ_i of the propagation paths slightly so that the total RF-phase shift at the measurement frequency is exactly the measured RF-phase ϕ_i.

7.3 Calculation of the frequency response from the measured multipath parameters

It is assumed that the measured delay-time of path i has a Normal distribution around the actual value with mean value τ_i and variance σ_i^2; from the radar analogy, as described in chapter 6 [Barton, 1969], this is reasonable. Another assumption that is made, is that the variance of the delay-time is constant for all paths, $\sigma_i^2 = \sigma^2$.
The delay-time distribution must be taken into account for the calculation of the power spectrum. The distribution function for the delay-time of a single path is given by:

$$p_{\tau_i}(\underline{t}) = 1/\sqrt{(2\pi\sigma^2)}\ \exp\{-(\underline{t}-\tau_i)^2/(2\sigma^2)\} \qquad (7.4)$$

Each delay-time τ_i is a stochastic variable now. With (7.4) we can calculate the probability density function $p_\tau(\underline{t})$ of each delay-time set $(\tau_1,\tau_2,..,\tau_N)$ chosen in the N-dimensional time space:

$$p_\tau(\underline{t}) = p_{\tau 1 \tau 2 \cdots \tau N}(\underline{t}_1,\underline{t}_2,\ldots,\underline{t}_N) = \prod_{i=1}^{N} p_{\tau i}(\underline{t}) \qquad (7.5)$$

Because of the uncertainty in the delay-times of the paths, also the power spectrum at a certain frequency will be distributed.
From each delay-time set the corresponding received power can be calculated with (7.2) for any frequency. The result is a power value g at frequency f with probability density $p_\tau(\underline{t})$. To obtain the power probability function $p_g(g)$ at constant frequency, we should add all probabilities $p_t(\underline{t})$ of the time sets $\underline{t}$ for which the power $g = S(f)$ has the same value:

$$p_g(\underline{g}) = \sum_{(S(f)|_{\underline{t}=\underline{t}} = g)} p_t(\underline{t}) \qquad (7.6)$$

With this method we can calculate the distribution of the power spectrum. For more detail on this point seen Appendix C.

With the help of a computer three typical values of the power spectrum are calculated:

1. the 90% value; this is the value of S(f) below which 90% of all calculated powers fall,
2. the mean value; this is the 50% value,
3. the 10% value.

In the figures 7.1a..c the three typical values of the power spectrum are given for the following situation:

1. Number of paths is 2
2. $A_1 = 1$; $A_2 = 0.842$
3. $\tau_1 = 0\ \mu s$; $\tau_2 = 0.972\ \mu s$
4. Delay-time standard deviation $\sigma = 6.38$ ns

The carrier frequency is 66 MHz.

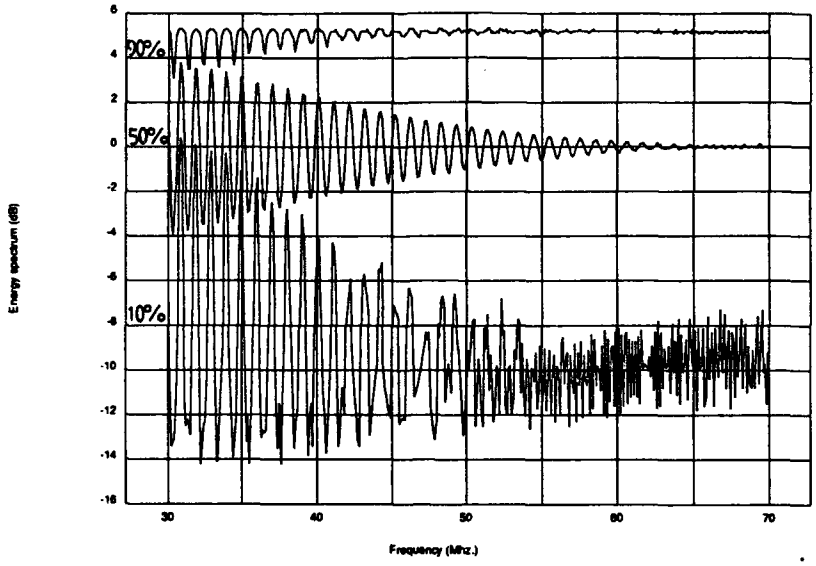

Fig. 7.1a: Frequency response 30 - 70 MHz

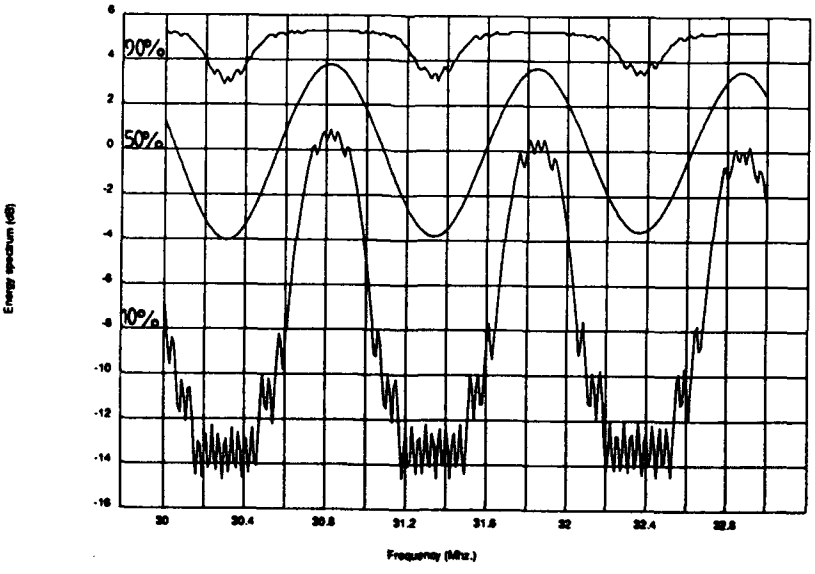

Fig. 7.1b: Frequency response 30 - 32.8 MHz

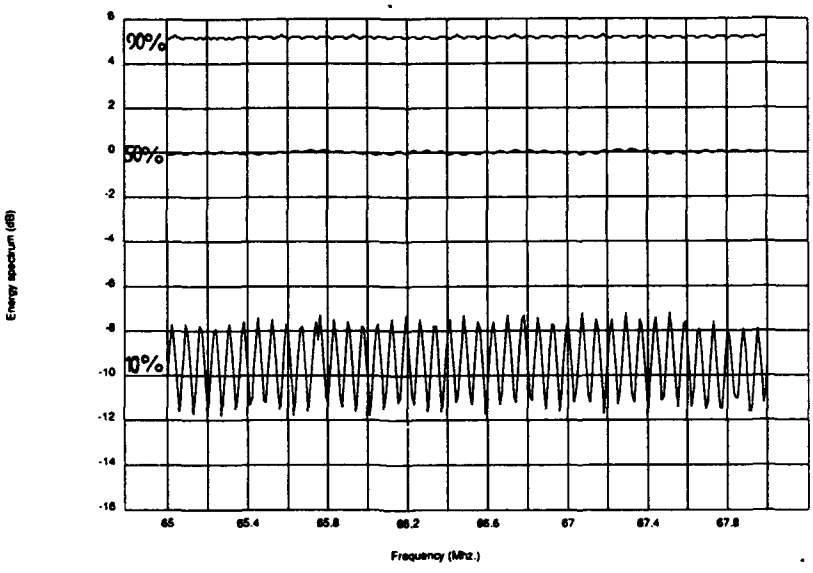

Fig. 7.1c: Frequency response 65 - 67.8 MHz

From the figures 7.1a..c it can be seen that at the higher frequencies there is a substantial gap between the 0.10 and 0.90 fraction curves. At lower frequencies, this difference becomes smaller. The gap depends on the frequency, since at higher frequencies the delay-time distribution causes greater differences in the argument of the sine and cosine functions of (7.2), whereas at lower frequencies the delay-time uncertainty causes a relatively small phase variation.
At a frequency of 70 MHz, a full period of 2π is reached already by a delay-time change of $\Delta\tau$ = 14.3 ns. Since this time is about twice the delay-time standard deviation, all possible power values between $(A_1 - A_2)^2$ = -16 dB and $(A_1 + A_2)^2$ = 5.3 dB will occur. Consequently there will be a great spread in the resulting power distribution at high frequencies. At the relatively low frequency of 30 MHz this is not the case, therefore the resulting power values will be more concentrated.

This method shows us that the measured delay-time differences are not accurate enough for calculating the relative RF-phase relations between the different paths over a wide frequency range.

However, the measured RF-phase values between the different paths are known at the measurement frequency. This information can be used to restrict the delay-time τ_i of path i to a relatively small number of discrete values. The RF-phase at frequency f for path i is:

$$\phi(f) = \phi_i - 2\pi f\tau_i \qquad (7.7)$$

Here ϕ_i is the measured RF-phase, which is the RF-phase at the measurement frequency, so τ_i is restricted by:

$$2\pi f_c\tau_i = 0 \qquad (7.8)$$

Now the probability density function of each delay-time becomes a discrete function. By a non-linear transformation the time variable τ_i is changed towards the nearest delay-times τ_i' that fulfills (7.8).
The time discretization is mathematically described by:

$$\tau_i' = [f_c\tau_i]/f_c \qquad (7.9)$$

With [x] is the integer so that $|x-[x]|$ is minimum and f_c is the carrier frequency of the measurement.
The probability of the resulting delay-times τ_i' is found by addition of all probability densities of the times that result in τ_i'. Figure 7.2 shows both the analogue and discrete delay-time distribution in case the radio channel consists of two paths.

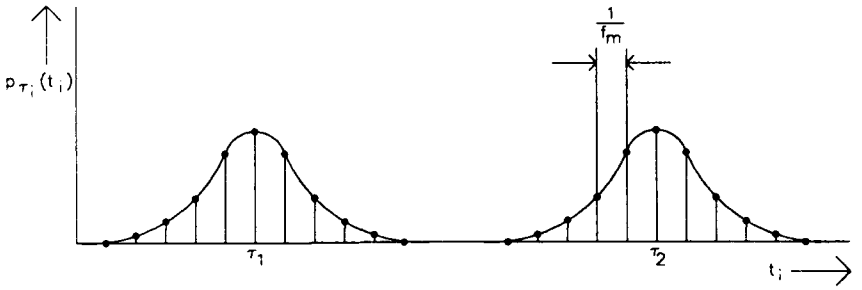

Fig. 7.2: Delay-time distribution function

Now the corrected delay-time τ_i' will result in the same RF-phase ϕ_i as measured for all times τ_i. Hence for this frequency the power density function consists of only one power component with value 1. For all other frequencies this is not the case. For different delay-times τ_i the corrected delay-times τ_i' result in a different power and again a power distribution will result, however, now it will be much less spread especially around the carrier frequency.

The same calculations as performed in figure 7.1 are now repeated for the case time discretization is applied. The results are shown in figures 7.3a..c.

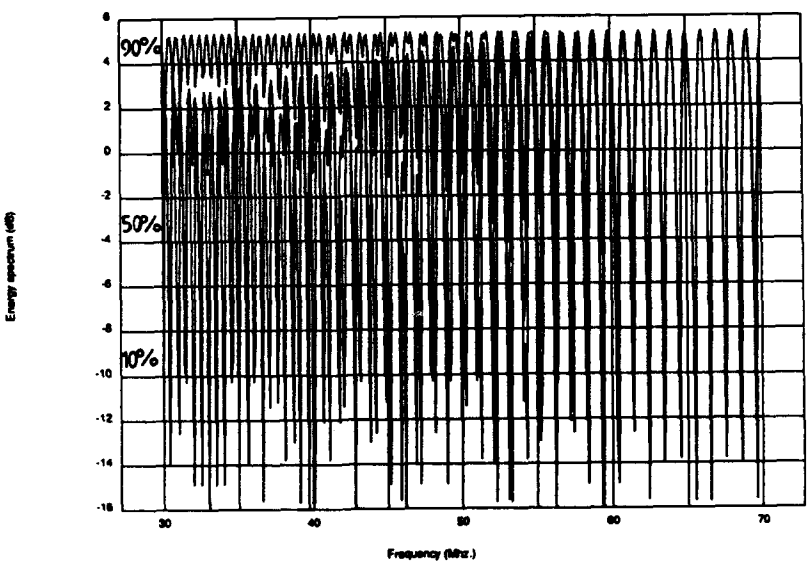

Fig. 7.3a: Frequency response 30 - 70 MHz, with time discretization

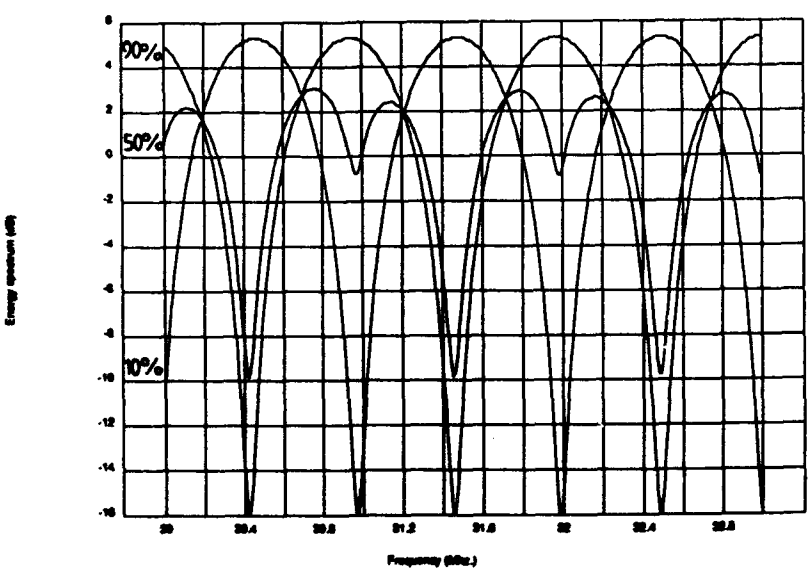

Fig. 7.3b: Frequency response 30 - 32.8 MHz, with time discretization

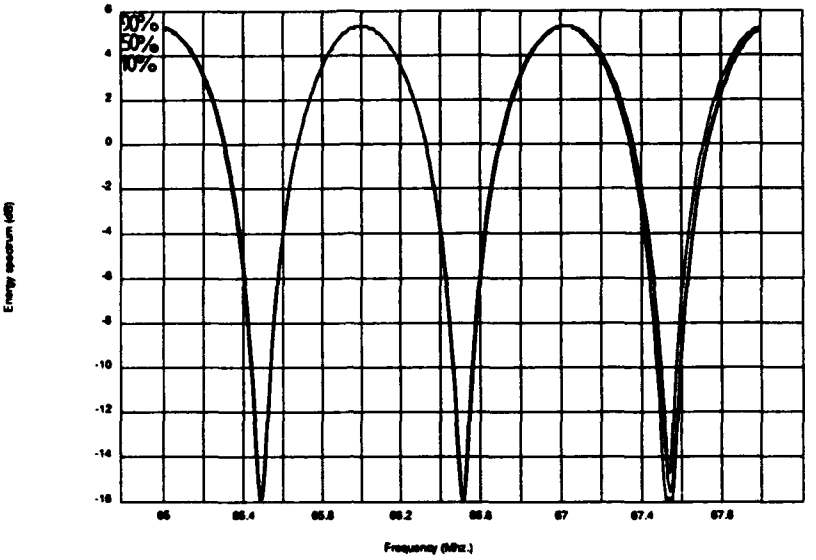

Fig. 7.3c: Frequency response 65 - 67.8 MHz, with time discretization

These figures show that the results are almost the same at relatively low frequencies. At high frequencies, however, the power distribution is completely different because of the time discretization. At the measurement frequency of f_c = 66 MHz there is no spread in the distribution as described in the foregoing. Starting from the measurement frequency, the power distribution becomes more spread.

7.4 Conclusion

Using the measured path parameters, the power spectrum of the frequency response can be calculated. The results are very accurate when the measured delay-times are slightly changed so that they are consistent with the measured relative RF-phases. These operations results in a number of discrete delay-time values for every path.

The calculated power spectrum is quite accurate over a much wider bandwidth than the bandwidth used for the measurements, however this is dependent on the delay-time accuracy.

8 RESULTS IN A SIMULATED MULTIPATH ENVIRONMENT

In this chapter the results of the measurement system operating in a controllable simulated multipath environment are discussed.

To determine the performance of the measurement system we have simulated a multipath environment. For a maximum number of three paths different amplitudes and delay-times can be manually adjusted. Also it is possible to add noise and other interference signals. For different configurations and at different frequencies measurements are performed. Upon data processing the results are compared with the chosen parameters.

8.1 Set-up of the simulated multipath environment

The block diagram of the simulated multipath environment is given in figure 8.1.

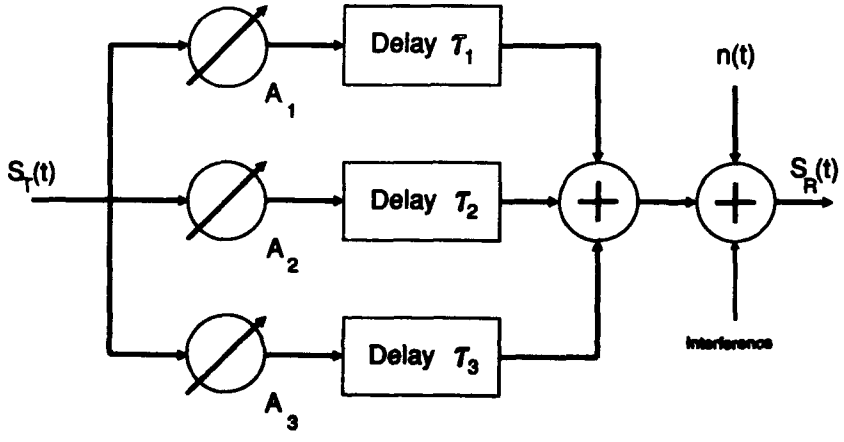

Fig. 8.1: Block-diagram of the simulated multipath radio channel

To simulate a path of the multipath radio channel we use an attenuator and a coaxial cable of certain length. The length of the cable determines the RF-phase and the delay-time. The cable length can vary up to about 300 m (≈ 1.5 μs). The exact delay-time of a cable is determined within an accuracy of +/- 6 ns. Delay-times varying from 0 to 1.5 μs can be realised in this way. The amplitude of each path is determined within +/- 1 dB ranging from 0 to -12 dB.

The different path responses are combined and additionally noise or an interference signal can be added. The noise power as well as the power and frequency of the jammer can be varied. All impedances are matched to avoid reflections in one and the same cable.

8.2 Measurements and results

The measurements are divided into four categories.

1. Accuracy
2. Addition of an interfering signal
3. Addition of noise
4. Measurement and calculation of the frequency response

8.2.1 Accuracy

For the first group of measurements the system is tested to determine the accuracy with which amplitude and delay-times are estimated. The noise power as well as the jammer power are zero. For equal configurations the measurements are executed at different frequencies spread over the VHF band. For one frequency the same measurement is executed a number of times (13) to examine the influence of time dependent parameters of the system. Results of the measurements can be found in the tables A.1 - A.11 of appendix A.

From these results it follows that the amplitudes relative to that of the strongest path, can be determined within +/- 2 dB for most cases. This corresponds with a maximal amplitude error ratio of $|A_{i,estimated}|/|A_{i,correct}| \approx 1.26$. The delay-times of the paths are determined with an accuracy of 2 sample instants to either side: $|\Delta\tau| \leq 2T_s = 31.25$ ns.

8.2.2 Addition of an interfering signal

For the second group of measurements, the influence of interference is examined. A jammer at a frequency separated 200 kHz from the carrier frequency is used to disturb the desired signal. The

signal power of the jammer signal is of the same order of magnitude as the desired signal. Results of the measurements are depicted in table A.12 of appendix A.

From these results we can conclude that the influence of the jammer can be neglected since it does not cause strong deviations from the configuration with no jammer present.

8.2.3 Addition of noise

If we add noise the same result is found as for addition of an interfering signal. Low input-SNR (down to 0 dB) do not influence the measurement results significantly. Results are depicted in table A.13 of appendix A.

8.2.4 Conversion of the results to the frequency response

The third multipath simulation includes the translation of the multipath characteristics to the frequency response, as described in chapter 7. For this measurement a configuration of three paths is simulated. Beside the direct path, two extra paths were used:

Path 1: $\tau_1 =$ 0 ns, $A_1 =$ 0 dB,
Path 2: $\tau_2 =$ 523 ns, $A_2 =$ 0 dB,
Path 3: $\tau_3 =$ 993 ns, $A_3 =$ -5.6 dB.

Three measurements were performed, each with a different path configuration: Paths 1 and 2, paths 1 and 3 and the configuration with all three paths. From the simulation algorithm the following result is determined:

Path 1: $\tau_1 =$ 0 ns, $A_1 =$ 0 dB, $\varphi_1 = 0^0$,
Path 2: $\tau_2 =$ 516 ns, $A_2 =$ -1 dB, $\varphi_2 = -77^0$,
Path 3: $\tau_3 =$ 1000 ns, $A_3 =$ -6 dB, $\varphi_3 = -155^0$.

Faults of the delay-time are due to time quantization. A standard deviation of $\sigma_1 = \sigma_2 = \sigma_3 = 18$ ns is used. This corresponds with the situation in which each of the delay-times is distributed uniformly over an interval of 3 times the sample time T_s ($3T_s = 47$ ns). Though the measurements were executed on the same frequencies as used in earlier experiments, the transformation results are described only for the case $f_c = 53.2$ MHz. For all other frequencies, the same results are found.

The results found are compared to the results found with an spectrum analyzer. Figures 8.2 through 8.7 show these results. From these it follows that for both the measurement results as well as the results obtained with the spectrum analyzer the same extremes in frequency and in magnitude of the energy spectra are found. If we take into account the measurement errors, we may conclude that the calculated energy spectrum of our system approximates the real situation very well.

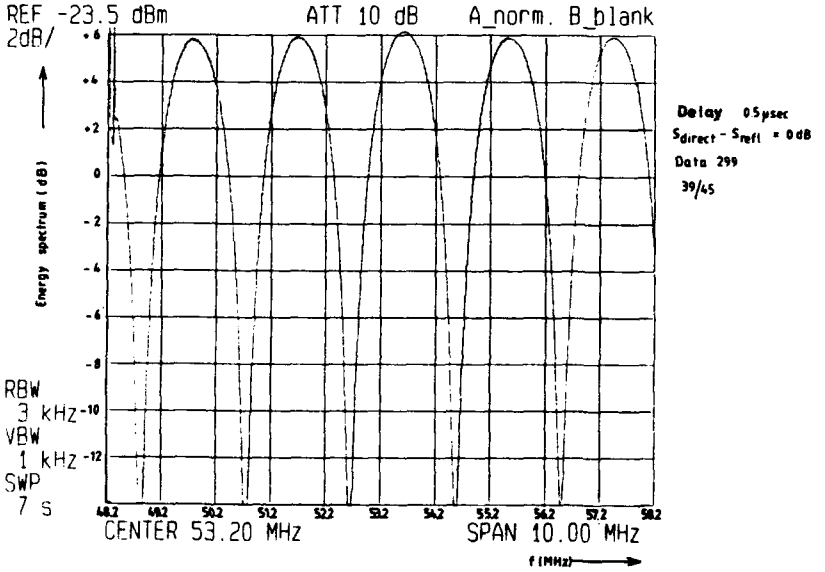

Fig. 8.2: Frequency response of the radio channel made of path 1 and path 2, results spectrum analysis

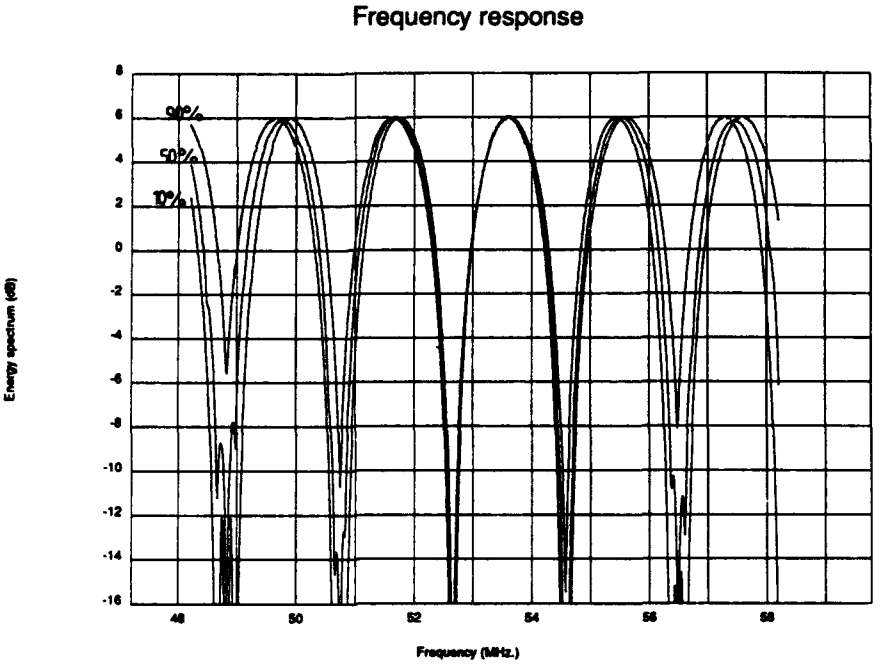

Fig. 8.3: Frequency response of the radio channel made of path 1 and path 2, estimation

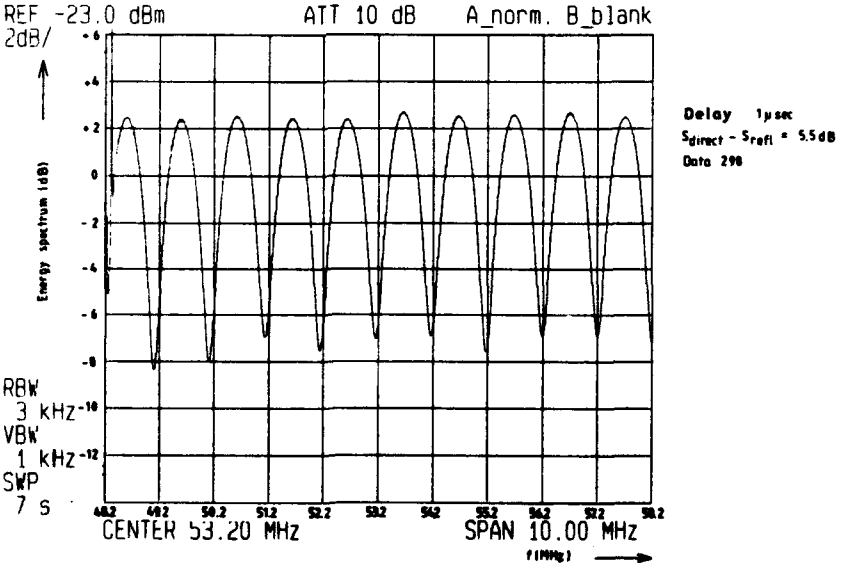

Fig. 8.4: Frequency response of the radio channel made of path 1 and path 3, results spectrum analysis

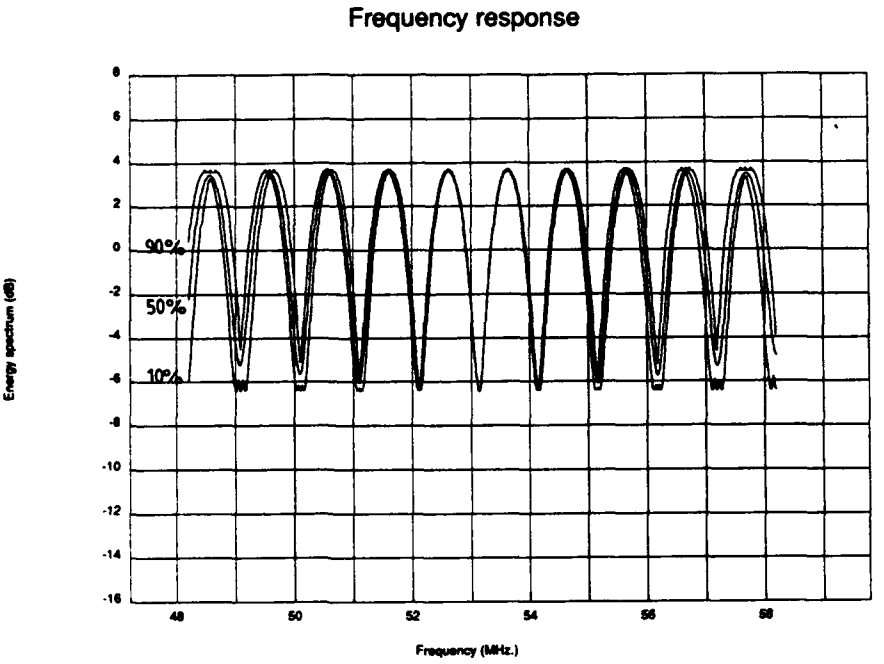

Fig. 8.5: Frequency response of the radio channel made of path 1 and path 3, estimation

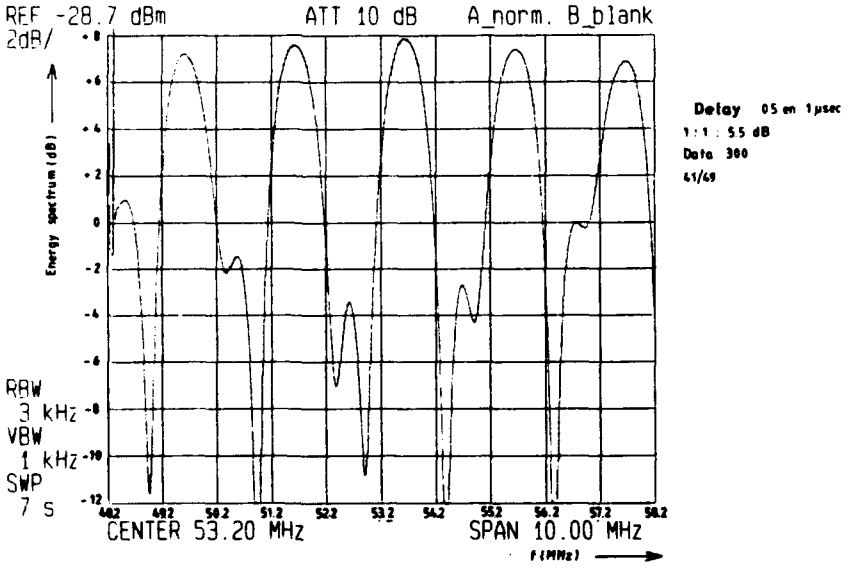

Fig. 8.6: Frequency response of the radio channel made of path 1, path 2, and path 3, results spectrum analysis

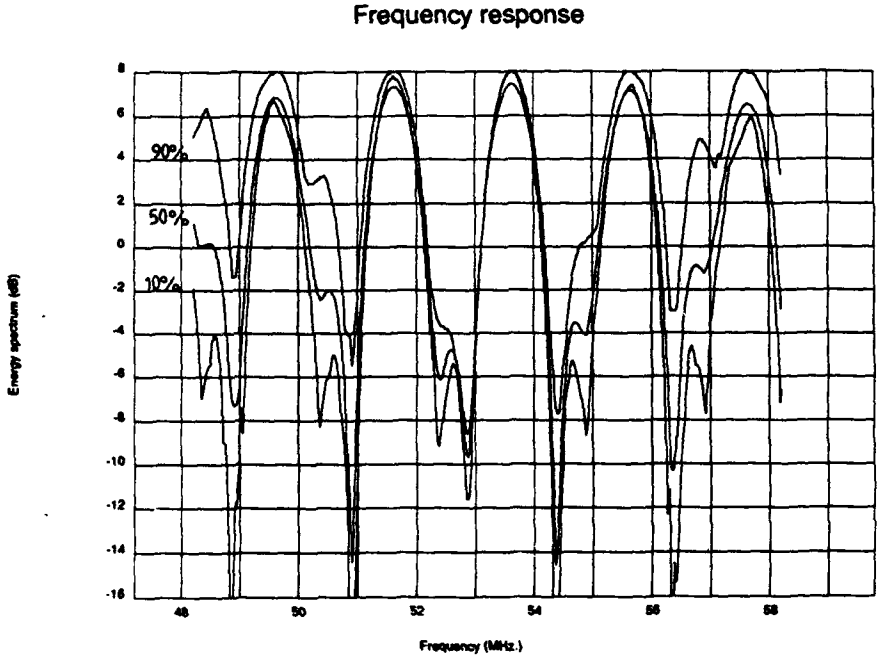

Fig. 8.7: Frequency response of the radio channel made of path 1, path 2 and path 3, estimation

CONCLUSIONS

To determine the multipath characteristics of a radio channel, a measurement system has been developed and implemented. This includes a transmitter-receiver configuration using Direct Sequence Spread Spectrum modulation. The frequency band of operation is the VHF-band, 30 - 70 MHz. Upon a measurement session, results are stored on disc. Software data processing leads to an estimate of the multipath characteristics.

From the theoretical evaluation and the measurement results obtained from a simulated multipath environment it follows that the multipath characteristics of a radio channel are completely described by the number of paths and their respective time-, phase- and delay-time differences.

Further it turns out that the technique presented, using a PN modulated carrier signal which is coherently detected at the receiver, serves best the goal to obtain the delay-times as well as the complex amplitudes of all paths in a multipath environment.
By using PN sequences the demands on power requirements of the transmitter are limited. Further, by processing a number of consecutive PN sequences it is feasible to increase the sample rate virtually by a factor equal to this number of sequences.

By applying a double correlation procedure, accurate results are obtained. At the first correlation stage, the received data is correlated with the PN sequence itself. In the second processing stage the obtained correlation function is correlated with the reference function.

The errors for each path due to noise for an input signal-to-noise ratio of SNR = -14 dB, are theoretically found to be:

- delay-time : 22 ns
- amplitude : 0.5 dB
- RF-phase : 3 degree;

Estimation of the multipath characteristics of a simulated multipath radio channel with known path delays and amplitude losses results for input-SNR = 0 dB in the following errors:

- delay-time : $\pm$ 7.8125 ns
- amplitude : $\pm$ 2 dB,

The multipath characteristics of the radio channel can be converted to the frequency domain. The narrowband frequency response of the radio channel is found within several dB's around the measurement frequency. Theoretical and measurement results of the narrowband frequency response of a simulated three path radio channel agree within ± 1 dB for a frequency band of 10 MHz centred around the measurement frequency.

LITERATURE

Abramowitz M., and Stegun, I.A.,
"Handbook of Mathematical Functions With Formulas. Graphs, and Mathematical Tables",
National Bureau of Standards, Washington, 1968.

Barton, D.K. and Ward, H.R.,
"Handbook of Radar Measurement",
Prentice Hall, London, 1969.

Benvenuto, N.,
"Distortion Analysis on Measuring the Impulse Response of a
System Using Crosscorrelation Method.",
AT&T Bell Laboratories Technical Journal, Vol.63, No.10, December 1984.

Carlson, A.B.,
"Communication systems", second edition,
McGraw-Hill Kogakusha Ltd., Tokyo, 1975.

Cox, Donald C.,
"Delay Doppler Characteristics of Multipath Propagation at 910 MHz in a
Suburban Mobile Radio Environment",
IEEE transactions on antennas and propagation, Vol. AP-20, No.5, September 1972.

Dixon, R.C.,
"Spread Spectrum Systems",
John Wiley & Sons, New York, 1976.

Feenstra, P.
"Een meetsysteem voor het bepalen van reflectieparameters bij radioverbindingen in de VHF-band."
FEL-90-B273, Fysisch en Electronisch Laboratorium TNO, 1990.

Holmes, J.K.,
"Coherent Spread Spectrum Systems",
John Wiley & Sons, New York, 1982.

Oppenheim, A.V. and Willsky, A.S.,
"Signals and Systems",
Prentice-Hall International, London, 1983.

Shanmugam, K.Sam,
"Digital and analog communication systems",
John Wiley & Sons, New York, 1979.

Vriens, J.A.M,
"Resultaten van de breedband-kanaalmetingen in rurale, heuvelachtige en stedelijke omgevingen",
Fysisch en Electronisch Laboratorium TNO, 1991.

Woodward, P.M.,
"Probability and Information Theory with Application to Radar",
Pergamon Press, 1953.

Ziemer, R.E. and Peterson, R.L.,
"Digital communnications and spread spectrum systems",
Macmillan Publishing Company, New York, 1985.

ABBREVIATIONS

A/D	: Analogue-Digital
A_c	: Carrier amplitude
a_k	: Contents of stage k of shift register
A_i	: Amplitude path i
b_k	: Symbol k of PN sequence
B_N	: Noise Bandwidth
D	: Number of sequences
E_p	: Pulse Energy
f_c	: Transmitter carrier frequency
h(t)	: Impulse response
I	: In-phase
K	: Sequence length
L	: Shift register length
M	: Number of samples per symbol
N	: Number of paths
N_0	: Noise spectral density
P	: Number of samples under consideration
PLL	: Phase Locked Loop
PN	: Pseudo-Noise
Q	: Quadrature phase
R	: Correlation function
R(τ)	: Continuous correlation function
R(m)	: Discrete correlation function
r	: Received signal
R_c	: Chip rate $1/T_c$
RF	: Radio Frequency
R_s	: Sample rate $1/T_s$
S	: Signal power
s	: Transmitted signal
SNR	: Signal to Noise Ratio
T	: Symbol duration
t	: Time

T_c	: Chip duration
T_s	: Sampling time
VHF	: Very High Frequency
Δ	: Error value
ϕ_i	: Phase shift of path i
σ^2	: Variance
τ_i	: Delay-time of path i
ω	: Radian frequency

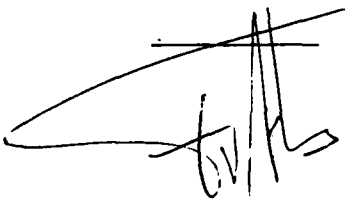

Ir. F.G.J. van Aken
(group leader)

Ir. G.J.M. Janssen
(author)

TABLES OF RESULTS FROM MEASUREMENTS IN THE SIMULATED MULTIPATH ENVIRONMENT

Configuration:

2 paths

Path 1: $t_1 = 0$ s $\quad A_1 = 0$ dB

Path 2: $t_2 = 523$ ns $\quad A_2 = 0$ dB

SNR = 40 dB

Table A.1: Measurement results

Frequency (MHz)	Delay-times (ns)		Amplitude (dB)	
	Correct	Measured	Correct	Measured
30.425	523	531	0	-4
39.975	523	516	0	-3
44.475	523	500	0	+1
49.825	523	531	0	-4
53.200	523	516	0	-1
70.925	523	516	0	-2

Configuration:

2 paths

Path 1: $t_1 = 0$ s $A_1 = 0$ dB

Path 2: $t_2 = 993$ ns $A_2 = 0$ dB

SNR = 40 dB

Table A.2: Measurement results

Frequency (MHz)	Delay-times (ns)		Amplitude (dB)	
	Correct	Measured	Correct	Measured
30.425	993	1016	0	-3
39.975	993	1016	0	+0
44.475	993	969	0	+0
49.825	993	1016	0	-1
53.200	993	1016	0	+2
70.925	993	938	0	+2

Configuration:

2 paths

Path 1: $t_1 = 0$ s $A_1 = 0$ dB

Path 2: $t_2 = 1516$ ns $A_2 = 0$ dB

SNR = 40 dB

Table A.3: Measurement results

Frequency (MHz)	Delay-times (ns)		Amplitude (dB)	
	Correct	Measured	Correct	Measured
30.425	1516	1484	0	-3
39.975	1516	1531	0	-2
44.475	1516	1516	0	+0
49.825	1516	1516	0	-6
53.200	1516	1516	0	+1
70.925	1516	1516	0	-4

Configuration:

2 paths

Path 1: $t_1 = 0$ s $A_1 = 0$ dB

Path 2: $t_2 = 523$ ns $A_2 = -4$ dB

SNR = 40 dB

Table A.4: Measurement results

Frequency (MHz)	Delay-times (ns)		Amplitude (dB)	
	Correct	Measured	Correct	Measured
30.425	523	500	-4	-2
39.975	523	547	-4	-4
44.475	523	531	-4	+1
49.825	523	516	-4	-2
53.200	523	516	-4	-2
70.925	523	516	-4	-6

Configuration:

2 paths

Path 1: $t_1 = 0$ s $A_1 = 0$ dB

Path 2: $t_2 = 993$ ns $A_2 = -4$ dB

SNR = 40 dB

Table A.5: Measurement results

Frequency (MHz)	Delay-times (ns)		Amplitude (dB)	
	Correct	Measured	Correct	Measured
30.425	993	1000	-4	-5
39.975	993	1016	-4	-3
44.475	993	984	-4	-3
49.825	993	1000	-4	-1
53.200	993	1000	-4	-6
70.925	993	1000	-4	-6

Configuration:

2 paths

Path 1: $t_1 = 0$ s $A_1 = 0$ dB

Path 2: $t_2 = 1516$ ns $A_2 = -4$ dB

SNR = 40 dB

Table A.6: Measurement results

Frequency (MHz)	Delay-times (ns)		Amplitude (dB)	
	Correct	Measured	Correct	Measured
30.425	1516	1531	-4	-3
39.975	1516	1516	-4	-3
44.475	1516	1500	-4	-5
49.825	1516	1516	-4	-4
53.200	1516	1531	-4	-4
70.925	1516	1531	-4	-5

Configuration:

2 paths

Path 1: $t_1 = 0$ s $A_1 = 0$ dB

Path 2: $t_2 = 523$ ns $A_2 = -10$ dB

SNR = 40 dB

Table A.7: Measurement results

Frequency (MHz)	Delay-times (ns)		Amplitude (dB)	
	Correct	Measured	Correct	Measured
30.425	523	547	-10	-12
39.975	523	516	-10	-6
44.475	523	516	-10	-16
49.825	523	547	-10	-12
53.200	523	500	-10	-11
70.925	523	531	-10	-10

Configuration:

2 paths

Path 1: $t_1 = 0$ s $A_1 = 0$ dB

Path 2: $t_2 = 993$ ns $A_2 = -10$ dB

SNR = 40 dB

Table A.8: Measurement results

Frequency (MHz)	Delay-times (ns)		Amplitude (dB)	
	Correct	Measured	Correct	Measured
30.425	993	969	-10	-10
39.975	993	1000	-10	-12
44.475	993	953	-10	-8
49.825	993	938	-10	-12
53.200	993	953	-10	-9
70.925	993	1031	-10	-8

Configuration:

2 paths

Path 1: $t_1 = 0$ s $A_1 = 0$ dB

Path 2: $t_2 = 1516$ ns $A_2 = -10$ dB

SNR = 40 dB

Table A.9: Measurement results

Frequency	Delay-times (ns)		Amplitude (dB)	
(MHz)	Correct	Measured	Correct	Measured
30.425	1516	1500	-10	-13
39.975	1516	1516	-10	-12
44.475	1516	1484	-10	-10
49.825	1516	1531	-10	-11
53.200	1516	1500	-10	-12
70.925	1516	1547	-10	-12

Configuration:

2 paths

Path 1: $t_1 = 0$ s $A_1 = 0$ dB

Path 2: $t_2 = 1516$ ns $A_2 = -10$ dB

SNR = 40 dB

Table A.10: Measurement results

Frequency (MHz)	Delay-times (ns)		Amplitude (dB)	
	Correct	Measured	Correct	Measured
53.200	1516	1516	-10	-13
53.200	1516	1516	-10	-13
53.200	1516	1531	-10	-13
53.200	1516	1531	-10	-11
53.200	1516	1531	-10	-11
53.200	1516	1531	-10	-11
53.200	1516	1531	-10	-11
53.200	1516	1531	-10	-11
53.200	1516	1500	-10	-11
53.200	1516	1500	-10	-11
53.200	1516	1516	-10	-11
53.200	1516	1500	-10	-11
53.200	1516	1516	-10	-11

Configuration:

3 paths

Path 1: $t_1 = 0$ s $A_1 = 0$ dB

Path 2: $t_2 = 523$ ns $A_2 = 0$ dB

Path 3: $t_3 = 993$ ns $A_3 = -5.6$ dB

SNR = 40 dB

Table A.11: Measurement results

Frequency	Delay-times (ns)		Amplitude (dB)	
(MHz)	Correct	Measured	Correct	Measured
30.425	523	516	0	-2
	993	938	-5.6	-8
39.975	523	516	0	-3
	993	1016	-5.6	-6
44.475	523	516	0	+3
	993	1016	-5.6	-6
49.825	523	531	0	-2
	993	969	-5.6	-8
53.200	523	516	0	-1
	993	969	-5.6	-6
70.925	523	547	0	-2
	993	984	-5.6	-7

Configuration:

2 paths

Path 1: $t_1 = 0$ s $A_1 = 0$ dB

Path 2: $t_2 = 1516$ ns $A_2 = 0$ dB

$f_{jammer} = 49.625$ MHz

$SNR_{jammer} = S_{PN}/S_{jammer} = ..$ dB

SNR = 40 dB (no jammer)

Table A.12: Measurement results

Frequency (MHz)	SNR_{jammer} (dB)	Delay-times (ns)		Amplitude (dB)	
		Correct	Measured	Correct	Measured
49.825	15	1516	1531	0	-2
49.825	10	1516	1531	0	-3
49.825	5	1516	1500	0	+15
49.825	*0*	*1516*	*1500*	*0*	-50

Configuration:

2 paths

Path 1: $t_1 = 0$ s $A_1 = 0$ dB

Path 2: $t_2 = 1516$ ns $A_2 = 0$ dB

SNR = .. dB

Table A.13: Measurement results

Frequency (MHz)	SNR_{jammer} (dB)	Delay-times (ns)		Amplitude (dB)	
		Correct	Measured	Correct	Measured
49.825	5	1516	1500	0	-5
49.825	5	1516	1500	0	-4
49.825	5	1516	1500	0	-3
49.825	5	1516	1500	0	-2
49.825	5	1516	1500	0	-2
49.825	5	1516	1531	0	-2
49.825	5	1516	1500	0	-4
49.825	5	1516	1484	0	-4
49.825	5	1516	1531	0	-3
49.825	5	1516	1484	0	-1
49.825	0	1516	1500	0	-3
49.825	0	1516	1500	0	-3
49.825	0	1516	1484	0	-6
49.825	0	1516	1484	0	-6
49.825	0	1516	1500	0	-4
49.825	0	1516	1500	0	-3
49.825	0	1516	1484	0	-3
49.825	0	1516	1500	0	-3
49.825	0	1516	1484	0	-4

Appendix B **Page B.1**

CALCULATION OF THE MULTIPATH CHARACTERISTICS

In (5.3) and (5.5) the expressions (4.31) and (4.32) for I[k] and Q[k] respectively can be substituted. By interchanging path addition and correlation we obtain the following expressions:

$$R_I[n] = \sum_{k=-\infty}^{\infty} \sum_{i=1}^{N} \{A_{ci} PN_{II}([n+k]T_{AD}-\tau_i) + A_{si} PN_{QI}([n+k]T_{AD}-\tau_i) + n_I([n+k]T_{AD})\}x[k] =$$

$$= \sum_{i=1}^{N} \sum_{k=-\infty}^{\infty} \{A_{ci} PN_{II}([n+k]T_{AD}-\tau_i) + A_{si} PN_{QI}([n+k]T_{AD}-\tau_i) + n_I([n+k]T_{AD})\}x[k] =$$

$$= \sum_{i=1}^{N} \sum_{k=-\infty}^{\infty} \{A_{ci} PN_{II}([n+k-l_i]T_{AD}) + A_{si} PN_{QI}([n+k-l_i]T_{AD}) + n_I([n+k]T_{AD})\}x[k] =$$

$$= \sum_{i=1}^{N} A_{ci} R_{II}[n-l_i] + A_{si} R_{QI}[n-l_i] + n_I[n], \qquad (B.1)$$

$$R_Q[n] = \sum_{i=1}^{N} -A_{si} R_{QQ}[n-l_i] + A_{ci} R_{IQ}[n-l_i] + n_Q[n]. \qquad (B.2)$$

In (B.1) and (B.2) the following definitions are used:

$$R_{II}[n] = \sum_{k=-\infty}^{\infty} PN_{II}([n+k]T_{AD})x[k], \qquad (B.3)$$

$$R_{QI}[n] = \sum_{k=-\infty}^{\infty} PN_{QI}([n+k]T_{AD})x[k], \qquad (B.4)$$

$$R_{IQ}[n] = \sum_{k=-\infty}^{\infty} PN_{IQ}([n+k]T_{AD})x[k], \qquad (B.5)$$

$$R_{QQ}[n] = \sum_{k=-\infty}^{\infty} PN_{QQ}([n+k]T_{AD})x[k], \qquad (B.6)$$

$$n_I[n] = \sum_{k=-\infty}^{\infty} n_I([n+k]T_{AD})x[k], \qquad (B.7)$$

$$n_Q[n] = \sum_{k=-\infty}^{\infty} n_Q([n+k]T_{AD})x[k], \qquad (B.8)$$

$$l_i = \mathrm{int}(\tau_i/T_{AD}) \qquad (B.9)$$

In (B.9) int(x) denotes the integer so that øx-int(x)ø is minimum. With this formula the analogue time τ_i is converted into the discrete time variable l_i. Note that the correlation functions $R_{II}[n]$, $R_{QI}[n]$, $R_{QI}[n]$ and $R_{QQ}[n]$ (which are called the reference correlation functions in chapter 5) are determined only by the system and are not dependent on the radio channel c.q. multipath characteristics itself. The correlation functions $R_{QI}[n]$ and $R_{IQ}[n]$ are due to cross-talk between the I- and Q-channels. These functions are used as reference functions to estimate the multipath characteristics. These reference functions are measured under laboratory conditions with the transmitter and receiver connected directly together.

From (B.1) and (B.2) we can see that the calculated correlation function is determined by

- the *multipath characteristics* N, A_{ci}, A_{si} and l_i for $i = 1,2,..,N$;
- the noise terms $n_I[n]$ and $n_Q[n]$;
- the system via $R_{II}[n]$, $R_{QI}[n]$, $R_{QI}[n]$ and $R_{QQ}[n]$.

We can now define the criterion for the data processing to estimate the multipath characteristics: Determine the number of paths (N) and for each path the amplitudes in the I- and Q-channel A_{ci}, A_{si} and delay-time l_i so that the energy contained in all estimates of the noise samples $n_I[n]$ and $n_Q[n]$ is minimum. In other words: find N, A_{ci}, A_{si} and l_i for i=1,2,..,N so that

$$\Delta^2 = \sum_{n=-\infty}^{\infty} \Delta[n]^2 = \Delta_I^2 + \Delta_Q^2 = \sum_{n=-\infty}^{\infty} \{\Delta_I[n]\}^2 + \sum_{n=-\infty}^{\infty} \{\Delta_Q[n]\}^2 =$$

$$= \sum_{n=-\infty}^{\infty} \{ R_I[n] - \sum_{i=1}^{N} A_{ci}R_{II}[n-l_i] + A_{si}R_{QI}[n-l_i] \}^2 +$$

$$+ \sum_{n=-\infty}^{\infty} \{ R_Q[n] - \sum_{i=1}^{N} -A_{si}R_{QQ}[n-l_i] + A_{ci}R_{IQ}[n-l_i] \}^2, \qquad (B.10)$$

is minimum. Since the energy of $R_I[n]$ and $R_Q[n]$ is concentrated in the peaks of the function only, the summation of (B.10) can be restricted to a limited number of P samples starting at p.

The parameters p and P must be determined first and differ for each radio channel. Any choice in which the P selected samples cover most energy of the correlation function satisfies but since the processing complexity linearly depends on P, the parameter should be chosen as small as possible.

An iterating algorithm is used to determine the multipath characteristics. The block structure of the algorithm is shown by the flowchart in figure B.1. The algorithm starts with N=1 paths and optimizes the amplitudes A_{c1} and A_{s1} and the delay-time l_1. From these parameters and the correlation functions $R_{II}[n]$, $R_{IQ}[n]$, $R_{QI}[n]$ and $R_{QQ}[n]$, the error Δ^2 of (B.10) is calculated. If this error Δ^2 exceeds a certain threshold the energy of the error function is supposed to originate from another path instead of the noise terms. In this case a following path is added and the algorithm starts over again to find the optimum solution for one extra path. Paths are added until the resulting error becomes less than the error threshold value Δ_{error}. The most important charts of the flowchart of figure B.1 will be described now.

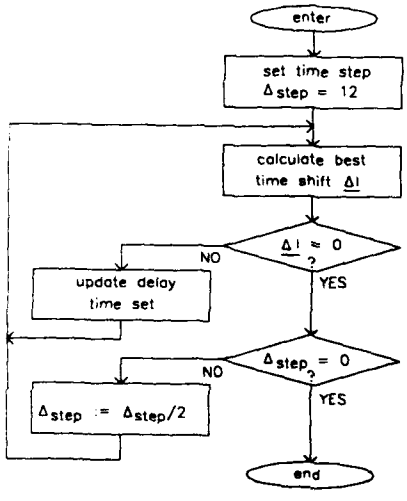

Fig. B.1: Flowchart of the algorithm

1 Delay-time determination

To determine the optimum amplitude and delay-time of an added path the algorithm starts by estimating the delay-time l_N. This time is determined from the error function $\Delta^2[n]$:

$$\Delta^2[n] = \{ R_I[n] - \sum_{i=1}^{N-1} A_{ci}R_{II}[n-l_i] + A_{si}R_{QI}[n-l_i] \}^2 + \\ + \{ R_Q[n] - \sum_{i=1}^{N-1} -A_{si}R_{QQ}[n-l_i] + A_{ci}R_{IQ}[n-l_i] \}^2. \quad (B.11)$$

The error function $\Delta^2[n]$ thus follows directly from the received samples ($R_I[n]$ and $R_Q[n]$) and the earlier estimated parameters A_{ci}, A_{si} and l_i for i = 1,2,..,N-1. From the error function $\Delta^2[n]$ the maximum $\Delta^2[m]$ is determined:

$$\Delta^2[m] \geq \Delta^2[n] \text{ for all } n, \quad (B.12)$$

with $n \in [p,p+P-1]$ and $m \in [p,p+P-1]$. The delay-time l_N is now chosen so that the reference correlation function $R_{II}^2[n-l_N]$ and $\Delta^2[n]$ have their maxima on the same instant. Note that l_N is a first estimate of the delay-time and may be changed by the following step of the algorithm.

2 Parameter optimization

The parameter optimization includes finding the best values for A_{si}, A_{ci} and l_i for i = 1,2,..,N-1,N. Note that the earlier found values for A_{si}, A_{ci} and l_i for i = 1,2,..,N-1 may be changed. The optimization consists of an iterating algorithm shown in figure B.2. The algorithm in principle consists of one step: the determination of the best time shift $\underline{\Delta l} = (\Delta l_1, \Delta l_2, .., \Delta l_N)$ relative to the current delay-time set $\underline{l} = (l_1, l_2, .., l_N)$. The magnitude of the time shift of the delay-time of one path can take on one of three values: $-\Delta_{step}$, 0 or $+\Delta_{step}$. The value of Δ_{step} changes upon program execution and depends upon the number of paths N. Initially $\Delta_{step} = 12$, $\Delta_{step} = 10$, $\Delta_{step} = 8$ ... for N = 1, N = 2, N = 3 ... paths. For this time shift all possible delay-time sets are formed by increasing and decreasing each delay element with the current delay step Δ_{step}. This results in N^3 delay-time sets: $(l_1-\Delta_{step}, l_2-\Delta_{step}, .., l_N-\Delta_{step})$, $(l_1-0, l_2-\Delta_{step}, .., l_N-\Delta_{step})$, $(l_1+\Delta_{step}, l_2-\Delta_{step}, .., l_N-\Delta_{step})$, .., $(l_1+\Delta_{step}, l_2+\Delta_{step}, .., l_N+\Delta_{step})$. For each delay-time set the optimum amplitudes $A_{c1}, A_{c2}, .., A_{cN}$ and $A_{s1}, A_{s2}, .., A_{sN}$ are calculated. This is accomplished by

setting the partial derivative of the error functions Δ_I^2 and Δ_Q^2 of (B.10) be equal to zero. By doing so, 2N equations must be solved to obtain the value of the 2N variables $A_{c1},A_{c2},...,A_{cN}$ and $A_{s1},A_{s2},...,A_{sN}$. For these values of the amplitude the error function (B.10) is minimum given the current delay-time set $\underline{l} = (l_1,l_2,...,l_N)$.

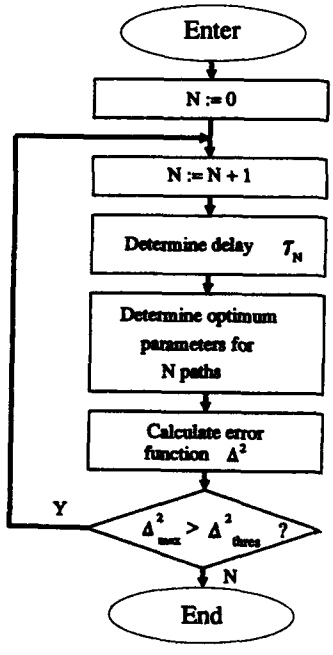

Fig. B.2: Flowchart on parameter optimization

The mathematical derivation of the foregoing is described now. The partial derivative of (B.10) relative to A_{cj} is given by:

$$\partial/\partial A_{cj} \sum_{n=p}^{p+P-1} \{\Delta[n]\}^2 = 0$$

$$\sum_{n=p}^{p+P-1} \partial/\partial A_{cj} \{\Delta_I[n]\}^2 + \sum_{n=p}^{p+P-1} \partial/\partial A_{cj} \{\Delta_Q[n]\}^2 = 0$$

$$\sum_{n=p}^{p+P-1} \{ \sum_{i=1}^{N} A_{ci}(R_{II}[n-l_i]R_{II}[n-l_j] + R_{IQ}[n-l_i]R_{IQ}[n-l_j]) +$$

$$\sum_{i=1}^{N} A_{si}(R_{QI}[n-l_i]R_{II}[n-l_j] - R_{QQ}[n-l_i]R_{IQ}[n-l_j]) +$$

$$- R_I[n]R_{II}[n-l_j] - R_Q[n]R_{IQ}[n-l_j]\} = 0. \quad (B.13)$$

For A_{sj} a similar result is found:

$$\partial/\partial A_{sj} \sum_{n=p}^{p+P-1} \{\Delta[n]\}^2 = 0$$

$$\sum_{n=p}^{p+P-1} \partial/\partial A_{sj} \{\Delta_I[n]\}^2 + \sum_{n=p}^{p+P-1} \partial/\partial A_{sj} \{\Delta_Q[n]\}^2 = 0$$

$$\sum_{n=p}^{p+P-1} \{ \sum_{i=1}^{N} A_{ci}(R_{II}[n-l_i]R_{QI}[n-l_j] - R_{IQ}[n-l_i]R_{QQ}[n-l_j]) +$$

$$\sum_{i=1}^{N} A_{si}(R_{QI}[n-l_i]R_{QI}[n-l_j] - R_{QQ}[n-l_i]R_{QQ}[n-l_j]) +$$

$$- R_I[n]R_{QI}[n-l_j] + R_Q[n]R_{QQ}[n-l_j]\} = 0. \quad (B.14)$$

We now define the inproduct elements:

$$A_{i,j} = \sum_{n=p}^{p+P-1} \{R_{II}[n-l_i]R_{II}[n-l_j] + R_{IQ}[n-l_i]R_{IQ}[n-l_j]\} \quad (B.15)$$

$$B_{i,j} = \sum_{n=p}^{p+P-1} \{R_{QI}[n-l_i]R_{II}[n-l_j] - R_{QQ}[n-l_i]R_{IQ}[n-l_j]\} \quad (B.16)$$

$$C_{i,j} = \sum_{n=p}^{p+P-1} \{R_{II}[n-l_i]R_{QI}[n-l_j] - R_{IQ}[n-l_i]R_{QQ}[n-l_j]\} \quad (B.17)$$

$$D_{i,j} = \sum_{n=p}^{p+P-1} \{R_{QI}[n-l_i]R_{QI}[n-l_j] + R_{QQ}[n-l_i]R_{QQ}[n-l_j]\} \quad (B.18)$$

$$E_j = \sum_{n=p}^{p+P-1} \{R_I[n-l_i]R_{II}[n-l_j] + R_Q[n-l_i]R_{IQ}[n-l_j]\} \quad (B.19)$$

$$F_j = \sum_{n=p}^{p+P-1} \{R_I[n-l_i]R_{QI}[n-l_j] - R_Q[n-l_i]R_{QQ}[n-l_j]\} \quad (B.20)$$

For (B.13) and (B.14) we can write:

$$\sum_{i=1}^{N} [A_{ci}\, A_{ij} + A_{si}\, B_{ij}] = E_j \text{ for } j = 1,2,..,N, \quad (B.21)$$

$$\sum_{i=1}^{N} [A_{ci}\, C_{ij} + A_{si}\, D_{ij}] = F_j \text{ for } j = 1,2,..,N. \quad (B.22)$$

The equations (B.21) and (B.22) can be written in matrix form for all j = 1,2,..,N:

$$\left(\begin{array}{ccccc|ccccc} A_{11} & A_{21} & \cdots & A_{N1} & & B_{11} & B_{21} & \cdots & B_{N1} & \\ A_{12} & A_{22} & \cdots & A_{N2} & & B_{12} & B_{22} & \cdots & B_{N2} & \\ \vdots & \vdots & & \vdots & & \vdots & \vdots & & \vdots & \\ A_{1N} & A_{2N} & \cdots & A_{NN} & & B_{1N} & B_{2N} & \cdots & B_{NN} & \\ \hline C_{11} & C_{21} & \cdots & C_{N1} & & D_{11} & D_{21} & \cdots & D_{N1} & \\ C_{12} & C_{22} & \cdots & C_{N2} & & D_{12} & D_{22} & \cdots & D_{N2} & \\ \vdots & \vdots & & \vdots & & \vdots & \vdots & & \vdots & \\ C_{1N} & C_{2N} & \cdots & C_{NN} & & D_{1N} & D_{2N} & \cdots & D_{NN} & \end{array}\right) \left(\begin{array}{c} A_{c1} \\ A_{c2} \\ \vdots \\ A_{cN} \\ \hline A_{s1} \\ A_{s2} \\ \vdots \\ A_{sN} \end{array}\right) = \left(\begin{array}{c} E_1 \\ E_2 \\ \vdots \\ E_N \\ \hline F_1 \\ F_2 \\ \vdots \\ F_N \end{array}\right) \quad (B.23)$$

The matrix equation (B.23) is solved by LU decomposition. With the results of the amplitudes $A_{c1},A_{c2},..,A_{cN}$ and $A_{s1},A_{s2},..,A_{sN}$, the error function of (B.10) is calculated. For one of the delay-time sets the error function is minimum. This result in the best delay-time shift and the new best delay-time set.

In case a different best time set results, $\underline{\Delta l} = (\Delta l_1,\Delta l_2,..,\Delta l_N) \neq (0,0,..,0)$, the algorithm continues by looking for the new best delay-time shift. In case the best delay-time shift set is zero for all shifts $(\Delta l_1,\Delta l_2,..,\Delta l_N) = (0,0,..,0)$ the algorithm continues depending on the shift step size Δ_{step}. If the shift step size is minimum, $\Delta_{step} = 1$, the algorithm ends and the current delay-time set $\underline{l}$ is the optimum delay-time set for N paths. In case $\Delta_{step} \neq 1$, the shift step size is decreased to be able to examine the intermediate delay-time sets.

The last step to obtain all multipath characteristics is the determination of the phase differences of the found paths. These follow directly from (4.19) and (4.20):

$$\phi_i = \arctan(A_{si}/A_{ci}). \qquad (B.24)$$

3 Complexity and convergence of the algorithm

- Complexity

Because the number of paths is of order of 5 for most cases, the complexity of the amplitude calculation is not determined by solving the matrix (B.23) but by the inproduct calculation (B.15) - (B.20). For each inproduct, 2P multiplications and P summations have to be calculated. For this reason the constant P, the number of sample instants under consideration, should be kept as small as possible.

- Convergence

The algorithm converges if the error Δ^2 decreases upon program execution. If the error Δ^2 is smaller than the threshold value $\Delta_{error}{}^2$, the algorithm ends. During program execution the error Δ^2 changes at two locations in the algorithm. First, if a new path is added and second if the delay-time set $\underline{l} = (l_1,l_2,..,l_N)$ is changed. Since changes in the delay-time set are determined by the error Δ^2 itself, the error will not increase upon optimization of the delay-time set.

The delay-time of a new extra path is determined by the maximum of the error function $\Delta^2[n]$ as described in section B.1. The new path causes a decrease of the error Δ^2 if the energy in the error function $\Delta^2[n]$ originates from a path of the radio channel. In case the energy of the error function is caused by noise, the change of the error Δ^2 is undetermined. In practice it turns out that the error Δ^2 decreases always. Hence we may state that the algorithm converges.

CALCULATION OF THE CUMULATIVE DISTRIBUTION FUNCTION OF THE FREQUENCY RESPONSE

From each delay-time set we can calculate the corresponding received power for any frequency with (7.2). The result is a power value g at frequency f with probability density $p_{\underline{\tau}}(\underline{t})$. To obtain the power probability density function $p_g(g)$ at constant frequency, we should add all probability density values $p_{\underline{\tau}}(\underline{t})$ of the time sets $\underline{t}$ for which the power $g = S(f)$ is equal:

$$p_g(g) = \sum_{(S(f)|_{\underline{\tau}=\underline{t}} = g)} p_{\underline{\tau}}(\underline{t}). \qquad (C.1)$$

Since we cannot determine the inverse function of (7.2) to calculate the time set $\underline{t}$ for a given power g, the power probability function $p_g(g)$ cannot be simplified further then as given according to formula (C.1). However, we can follow a statistical approach for which we do not need this inverse function. For instance, at frequency f, the mean power $E[g|f]$ can be calculated by:

$$E[g|f] = \int_{-\infty}^{\infty} \cdots \int_{-\infty}^{\infty} S(f)|_{\underline{\tau}=\underline{t}} \; p_{\underline{\tau}}(\underline{t}) \; dt_1 dt_2 \cdots dt_N. \qquad (C.2)$$

With the aid of computer calculations, we can approximate (C.1). To do so, we quantify the variables g and $\underline{\tau}$. The time intervals are chosen small enough so that the energy spectrum S(f) for all delay-times within the intervals differs only slightly. The time scales are regarded further only for the area with substantial probability density of the delay-time. If we restrict the time scale of each delay-time to the interval $[\tau_i-2\sigma, \tau_i+2\sigma]$, a fraction of 0.95 is covered. This scale is divided into M intervals of equal length. The probability p_j of the delay-time τ_i to fall in the interval j, $\tau_i \in [\tau_i-2\sigma+4\{j-1\}\sigma/M, \tau_i-2\sigma+4\{j\}\sigma/M]$ for j=1,2,..,M, is calculated with the Q-function:

$$p_j = \int_{\tau_i-2\sigma+4(j-1)\sigma/M}^{\tau_i-2\sigma+4j\sigma/M} p_\tau(t)\,dt =$$

$$= Q(-2+(j-1)/M) - Q(-2+j/M), \qquad (C.3)$$

with

$$Q(x) = \int_x^\infty 1/\sqrt{(2\pi)}\ \exp(-y^2/2)\ dy. \qquad (C.4)$$

The Q-function is well tabulated or can be calculated by function approximation (Abramowitz, M. and Stegun, I.A., 1968). For N paths this method leads to M^N delay-time sets. For each delay-time set the corresponding power value (or power g) is calculated from (7.2). The resulting powers are tabulated and an approximation of (C.1) is obtained.

UNCLASSIFIED

REPORT DOCUMENTATION PAGE (MOD-NL)

1. DEFENSE REPORT NUMBER (MOD-NL)	2. RECIPIENT'S ACCESSION NUMBER	3. PERFORMING ORGANIZATION REPORT NUMBER
TD91-2012		FEL-91-B112

4. PROJECT/TASK/WORK UNIT NO.	5. CONTRACT NUMBER	6. REPORT DATE
20420		JUNE 1991

7. NUMBER OF PAGES	8. NUMBER OF REFERENCES	9. TYPE OF REPORT AND DATES COVERED
100 (INCL. 3 APPENDICES + RDP, EXCL. DISTRIBUTION LIST)	13	FINAL

10. TITLE AND SUBTITLE
RADIO CHANNEL MEASUREMENTS USING A BROADBAND PSEUDO-NOISE SIGNAL (MEASUREMENT SET-UP AND PROCESSING OF THE RESULTS)

11. AUTHOR(S)
IR. J.A.M. VRIENS, IR. G.J.M. JANSSEN

12. PERFORMING ORGANIZATION NAME(S) AND ADDRESS(ES)
TNO PHYSICS AND ELECTRONICS LABORATORY, P.O. BOX 96864, 2509 JG THE HAGUE
OUDE WAALSDORPERWEG 63, THE HAGUE, THE NETHERLANDS

13. SPONSORING/MONITORING AGENCY NAME(S)
TNO PHYSICS AND ELECTRONICS LABORATORY,
THE HAGUE, THE NETHERLANDS

14. SUPPLEMENTARY NOTES
THE PHYSICS AND ELECTRONICS LABORATORY IS PART OF THE NETHERLANDS ORGANIZATION FOR APPLIED SCIENTIFIC RESEARCH

15. *ABSTRACT (MAXIMUM 200 WORDS, 1044 POSITIONS)*
IN A MULTIPATH COMMUNICATIONS ENVIRONMENT, WHICH IS OFTEN FOUND IN URBAN AREAS, TRANSMISSION OF INFORMATION IS DIFFICULT DUE TO SELF-INTERFERENCE. THIS SELF-INTERFERENCE MAY RESULT IN SIGNAL SUPPRESSION AND INTERSYMBOL INTERFERENCE. KNOWLEDGE OF THE PARAMETERS THAT CHARACTERIZE THE RADIO CHANNEL, CAN BE USED TO FEED AN ADAPTIVE EQUALIZER OR FREQUENCY MANAGEMENT SYSTEM, IN ORDER TO MINIMIZE THESE DISTURBING EFFECTS. IN THIS REPORT A MEASUREMENT SYSTEM, TO MEASURE THE CHARACTERISTICS OF RADIO PATHS IN A MULTIPATH CHANNEL, IS DESCRIBED AND MEASUREMENT RESULTS ARE GIVEN. THE MEASUREMENT SYSTEM USES PSEUDO-NOISE SPREAD SPECTRUM MODULATION AND OPERATES IN THE VHF-BAND (30 - 70 MHZ). A CARRIER, BPSK MODULATED WITH THE PSEUDO-NOISE SIGNAL AT A RATE OF 1 MCHIP/S, IS USED TO SOUND THE RADIO CHANNEL. THE CHARACTERISTICS OF THE DIFFERENT RADIO PATHS: RELATIVE AMPLITUDE, RF-PHASE AND DELAY-TIME, ARE CALCULATED FROM THE COHERENTLY RECEIVED SIGNAL.
THE ACCURACY OF THE MEASUREMENT SYSTEM HAS BEEN DETERMINED AND IS: 2 DB FOR THE AMPLITUDE, 5^{O} FOR THE RF-PHASE AND 20 NS FOR THE DELAY-TIME. WITH THE SYSTEM MEASUREMENTS HAVE BEEN PERFORMED IN A CONTROLLED MULTIPATH ENVIRONMENT IN THE LABORATORY AND IN THE FIELD IN DIFFERENT TYPES OF TERRAIN. THE CONTROLLED MULTIPATH RESULTS ARE PRESENTED IN THIS REPORT, THE ANALYSIS OF THE MEASUREMENTS PERFORMED IN DIFFERENT TYPES OF TERRAIN WILL BE PRESENTED IN (VRIENS, 1991).

16. DESCRIPTORS	IDENTIFIERS
MULTIPATH PROPAGATION MEASUREMENT	RADIO CHANNEL CHARACTERISTICS AMPLITUDE DELAY TIME RF PHASE

17a. SECURITY CLASSIFICATION (OF REPORT)	17b. SECURITY CLASSIFICATION (OF PAGE)	17c. SECURITY CLASSIFICATION (OF ABSTRACT)
UNCLASSIFIED	UNCLASSIFIED	UNCLASSIFIED

18. DISTRIBUTION/AVAILABILITY STATEMENT	17d. SECURITY CLASSIFICATION (OF TITLES)
UNLIMITED	UNCLASSIFIED

UNCLASSIFIED

Distributielijst

1.	Hoofddirecteur van de Hoofdgroep Defensieonderzoek TNO
2.	Directeur Wetenschappelijk Onderzoek en Ontwikkeling
3.	HWO-KL
4. + 5.	HWO-KLu
6.	HWO-KM
7.	
t.m.	Hoofd TDCK
9.	
10.	DMKL/CIS, t.a.v. Ikol. G. Hoevenaars
11.	CVKL/TEA-1, t.a.v. maj. G. Kanis
12.	CVKL/TEA-1, t.a.v. kapt. M.H.L.J. van Bokkel
13.	CVKL/TEA-3, t.a.v. maj. ir. H.G. Oude Lohnis
14.	CVKL/TEA-5, t.a.v. maj. J.A.C. van de Weel
15.	Technische Universiteit Delft, Vakgroep Telecommunicatie en Verkeersbegeleidingssystemen, t.a.v. prof. R. Prasad
16.	Directie FEL-TNO, ir. P. Spohr
17.	Directie FEL-TNO, dr. J.W. Maas, daarna reserve
18.	Archief FEL-TNO, in bruikleen aan ir. G.H. Heebels
19.	Archief FEL-TNO, in bruikleen aan ir. F.G.J. van Aken
20.	Archief FEL-TNO, in bruikleen aan ir. P.J. van Vliet
21.	Archief FEL-TNO, in bruikleen aan ir. M.A.A. Melters
22.	Archief FEL-TNO, in bruikleen aan P. Feenstra
23.	Archief FEL-TNO, in bruikleen aan ir. G.J.M. Janssen
24.	Documentatie FEL-TNO
25.	Reserve

Indien binnen de leiggemacht extra exemplaren van dit rapport worden gewenst door personen of instanties die niet op de verzendlijst voorkomen, dan dienen deze aangevraagd te worden bij het betreffende Hoofd Wetenschappelijk Onderzoek of, indien het een K-opdracht betreft, bij de Directeur Wetenschappelijk Onderzoek en Ontwikkeling.